

AD-A070 430

NAVAL WEAPONS CENTER CHINA LAKE CA

F/6 9/1

INTEGRATED OPTICS.(U)

DEC 75 L D HUTCHESON

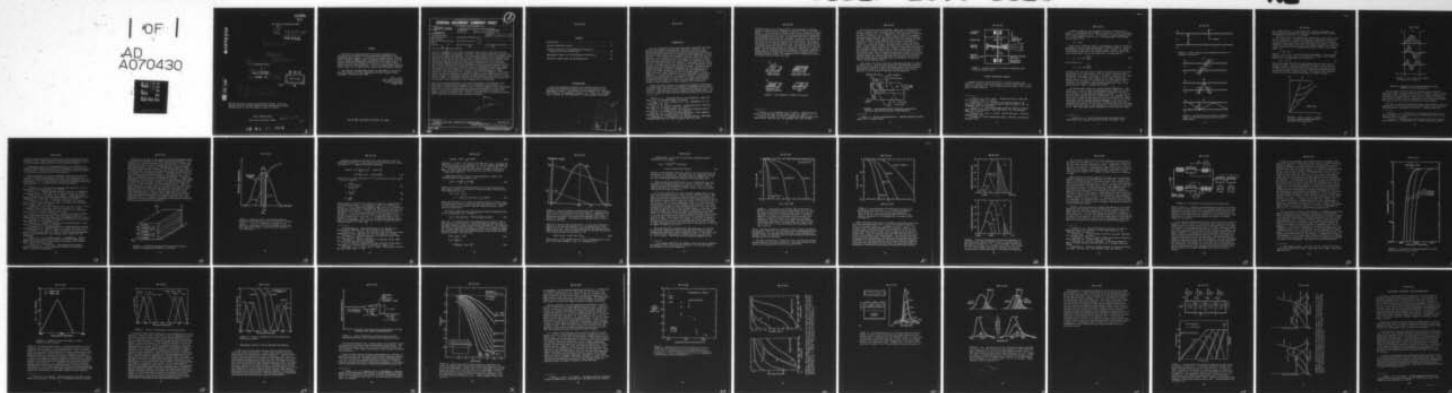
UNCLASSIFIED

NWC-TM-2592

61DEP-E099-1628

NL

1 OF 1
AD
A070430



END

DATE

FILMED

8-79

DDC

ADA070430

DDC FILE COPY

102886
Ncl

NWC Technical Memorandum 2592

①
LEVEL H

⑭ NWC-TM-2592

⑮ GIDEP

⑰ E499-1828

⑥ INTEGRATED OPTICS .

by

⑩ L. D. Hutcheson
Research Department

⑪ DECEMBER 1975

⑫ 40p.

DDC

RECEIVED
JUN 26 1979

A

⑨ Technical memo.
Jul 73 - Jun 75

Approved for public release; distribution unlimited. This is an informal report of the Naval Weapons Center containing preliminary information and is not to be used as a basis for action.

NAVAL WEAPONS CENTER

China Lake, California 93555

403 019

LB

79 01 11 079

FOREWORD

This report has been prepared for the timely presentation of information on the analytical and experimental development of the integrated optics program. In particular it presents results obtained both at the Naval Weapons Center and elsewhere which apply to a multiplexing scheme for communication purposes on a fiber optic bundle. It reports on preliminary findings of the study and is released at the working level for information only. This is an interim report and additional reports will be published as research and development continues.

This research and development effort was performed for the period July 1973 through June 1975, supported by the Naval Weapons Center independent research project funds.

Fred C. Essig
Head, Physics Division
Research Department
1 August 1975

26 APR 1978

GOVERNMENT-INDUSTRY DATA EXCHANGE PROGRAM

GENERAL DOCUMENT SUMMARY SHEET

1 OF 1

Please Type All Information - See Instructions on Reverse

1. ACCESS NUMBER E099-1828		2. COMPONENT/PART NAME PER GIDEP SUBJECT THESAURUS Optoelectronic Devices, Optical Coupler	
3. APPLICATION Engineering		4. MFR NOTIFICATION <input type="checkbox"/> NOTIFIED <input checked="" type="checkbox"/> NOT APPLICABLE	5. DOCUMENT ISSUE (Month/Year) December 1975
6. ORIGINATOR'S DOCUMENT TITLE Integrated Optics		7. DOCUMENT TYPE <input checked="" type="checkbox"/> GEN RPT <input type="checkbox"/> NONSTD PART <input type="checkbox"/> SPEC	
8. ORIGINATOR'S DOCUMENT NUMBER NWC TM 2592	9. ORIGINATOR'S PART NAME/IDENTIFICATION N/A		
10. DOCUMENT (SUPERSEDES) (SUPPLEMENTS) ACCESS NO. None	11. ENVIRONMENTAL EXPOSURE CODES N/A		
12. MANUFACTURER N/A	13. MANUFACTURER PART NUMBER N/A	14. INDUSTRY/GOVERNMENT STANDARD NUMBER N/A	

15. OUTLINE, TABLE OF CONTENTS, SUMMARY, OR EQUIVALENT DESCRIPTION

The term "integrated optics" came into being 6 years ago but since that time the number of governmental, industrial, university, and research laboratories involved in this field has grown and ramified. For the interested reader there is available a good collection of survey articles which review both the progress and the fundamentals of this new field. Like integrated electronics, integrated optics (IO) does not really provide new possibilities in principle, but it makes practical many well-known applications that would remain too cumbersome or expensive to be utilized without this technique. Traditional optical apparatus must be aligned with extreme accuracy and is thus susceptible to the smallest amount of vibration and temperature change. Integrated optics concentrates light in thin-film waveguides that are deposited on the surface or inside a substrate. Because of the short wavelength of light, dielectric light waveguides can be extremely small in their dimensions. The reduced size of IO circuits thus makes it possible to achieve a much higher density of components compared to conventional optical equipment aligned on steel rails or on heavy optical benches. An additional advantage of the small size and rugged construction of dielectric light waveguides is their insensitivity to vibrations.

This report has been prepared for the timely presentation of information on the analytical and experimental development of the integrated optics program. In particular it presents results obtained both at the Naval Weapons Center and elsewhere which apply to a multiplexing scheme for communication purposes on a fiber optic bundle. It reports on preliminary findings of the study and is released at the working level for information only. This is an interim report and additional reports will be published as research and development continues.

Ref. Tome

16. KEY WORDS FOR INDEXING Waveguide; Data Link; Transmission; Integrated Optics		(Doc Des--M)
17. GIDEP REPRESENTATIVE M. H. Sloan	18. PARTICIPANT ACTIVITY AND CODE Naval Weapons Center, China Lake (X7)	

DD FORM 1 OCT 77 2000

REPRODUCTION OR DISPLAY OF THIS MATERIAL FOR
SALES OR PUBLICITY PURPOSES IS PROHIBITED

40

CONTENTS

Introduction	3
Optical Waveguiding Concepts	6
Analytical Aspects of Electroabsorption Modulator/ Detector for Color Multiplexing	10
Experimental Aspects of the EA Modulator and Detector	27
Discussion, Conclusions, and Recommendations	38

ACKNOWLEDGMENT

The author expresses gratitude to Dr. Nicholas Bottka for his intuitive and informative insights into both the theoretical and experimental studies. Appreciation is also extended to Dr. John Rahn for his work on the temperature studies. Dr. M. Scott, Dr. R. Hughes, and J. Jernigan are also appreciated for their valuable discussions.

Accession For	
NTIS GRA&I	<input checked="" type="checkbox"/>
DDC TAB	<input type="checkbox"/>
Unannounced	<input type="checkbox"/>
Justification	
By _____	
Distribution/	
Availability Codes	
Dist.	Avail and/or special
A	

INTRODUCTION

The term "integrated optics" came into being 6 years ago¹ but since that time the number of governmental, industrial, university, and research laboratories involved in this field has grown and ramified. For the interested reader there is available a good collection of survey articles²⁻⁶ which review both the progress and the fundamentals of this new field. Like integrated electronics, integrated optics (IO) does not really provide new possibilities in principle, but it makes practical many well-known applications that would remain too cumbersome or expensive to be utilized without this technique. Traditional optical apparatus must be aligned with extreme accuracy and is thus susceptible to the smallest amount of vibration and temperature change. Integrated optics concentrates light in thin-film waveguides that are deposited on the surface or inside a substrate. Because of the short wavelength of light, dielectric light waveguides can be extremely small in their dimensions. The reduced size of IO circuits thus makes it possible to achieve a much higher density of components compared to conventional optical equipment aligned on steel rails or on heavy optical benches. An additional advantage of the small size and rugged construction of dielectric light waveguides is their insensitivity to vibrations.

Integrated optics involves the technology of guiding and manipulating optical waves in dielectric waveguides, the generation and detection of optical waves, and the coupling of optical waves into and out of IO circuits. Integrated optics can be divided into two general areas. The first is passive IO, which involves coupling, guiding, and partitioning

¹ Miller, S. E. "Integrated Optics: An Introduction," BELL SYST TECH J, Vol. 48 (September 1969), pp. 2059-69.

² Goell, J. E., R. D. Standley, and T. Li. ELECTRONICS, Vol. 20 (August 1970), pp. 60-67.

³ Goell, J. E., and R. D. Standley. "Integrated Optical Circuits," PROC IEEE, Vol. 58 (October 1970), pp. 1504-12.

⁴ Tien, P. K. "Light Waves in Thin Films and Integrated Optics," APPL OPT, Vol. 10 (November 1971), pp. 2395-2413.

⁵ Miller, S. E. "A Survey of Integrated Optics," IEEE J QUANTUM ELECTRON, Vol. QE-8 (February 1972), pp. 199-205.

⁶ Kogelnik, H. "An Introduction to Integrated Optics," IEEE TRANS MICROWAVE THEOR TECH, Vol. MTT-23 (January 1975), pp. 2-20.

of optical waves in IO circuits without the application of external fields or acoustic waves. Examples of passive IO circuits are shown in Figure 1. The prism coupler⁷ couples light into the waveguide by means of the evanescent electric field of the prism which has an exponential tail extending below the prism. The waveguide mode has an exponential tail extending upward above the waveguide. These two exponential tails overlap in the air gap between the prism and waveguide. The parts of the fields that overlap are common to the prism and the film waveguide and constitute the coupling between them. The grating coupler acts as a standard diffraction grating to couple light into and out of the waveguide. The directional coupler is a means of coupling all or partial energy from one waveguide to another waveguide. The energy transfer is accomplished in the same manner as with the prism coupler, which is through evanescent fields. The waveguide lens⁸ is formed by a refractive index variation across the film.

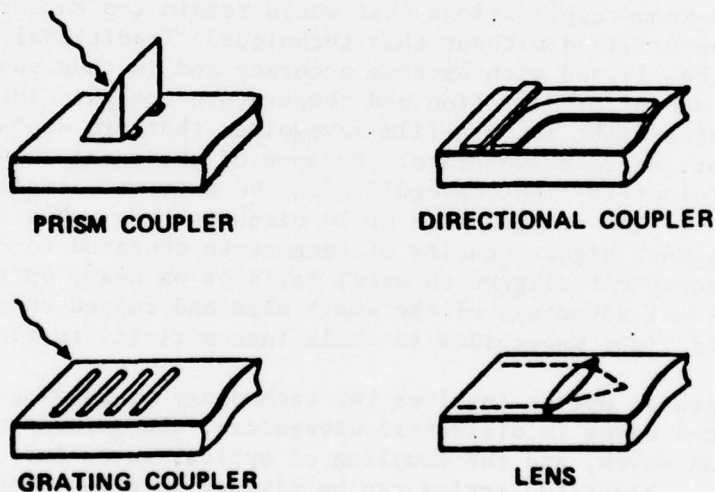


FIGURE 1. Four Examples of Passive IO Circuits.

⁷ Harris, J. H., R. Shubert, and J. N. Polky. "Beam Coupling of Films," J OPT SOC AMER, Vol. 60 (August 1970), pp. 1007-16.

⁸ Ulrich, R., and R. J. Martin. "Geometrical Optics in Thin Film Light Guides," APPL OPT, Vol. 10 (September 1971), pp. 2077-85.

The second area, active IO circuits, makes use of applied electric fields or acoustic waves to provide for the modulation, deflection, variable coupling, etc., of optical waves. Two such active IO circuits are shown in Figures 2 and 3. Figure 2 shows a dielectric waveguide incorporating an injection laser and an electro-optic phase modulator.⁹ The light coupled from the injection laser into the waveguide is modulated by an electric field which causes a change in the index of refraction. Since the phase of the optical wave is directly proportional to the refractive index, this then leads to modulation of the phase. Figure 3 shows an active IO circuit in which light is diffracted by a traveling surface acoustic wave. Light is coupled into the thin film through a grating coupler very much like the one shown in Figure 1. The acoustic wave, which is produced by applying a voltage to the interdigital transducers, forms a phase grating which diffracts the light in the same manner as a transmission diffraction grating. Both the diffracted and the undiffracted light wave are coupled out of the thin film by another grating coupler.

This report will first review the principles which lead to guiding of optical waves. Then both the theoretical and experimental results that have been achieved at the Naval Weapons Center will be presented. Experimental results of another research laboratory which pertain directly to the IO project at NWC will also be presented.

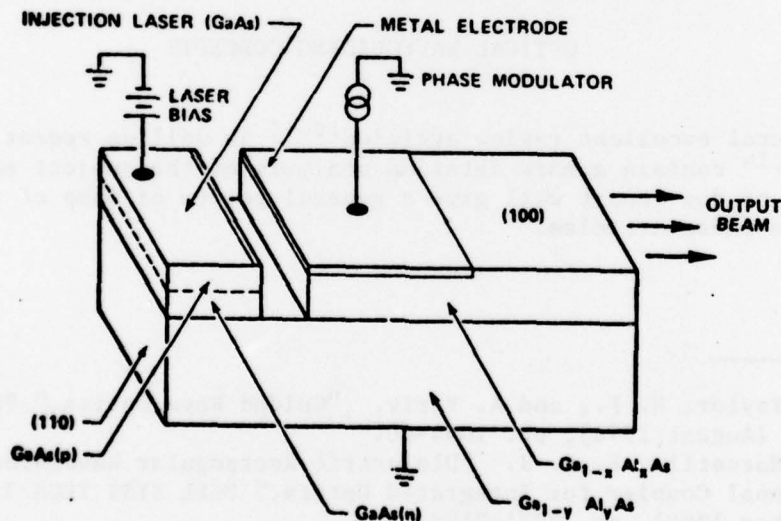


FIGURE 2. $\text{Ga}_{1-x}\text{Al}_x\text{As}$ Dielectric Waveguide Incorporating Injection Laser and Electro-optic Phase Modulator.

⁹ Yariv, A. "Active Integrated Optics." Advanced Research Projects Agency TR 1-71 (August 1971).



8

8

8

- 8

A planar asymmetric slab waveguide structure is illustrated in Figure 4. The waveguide has an index of refraction n_1 , with surrounding media having indices n_0 and n_2 . The structure is called symmetric when $n_0 = n_2$ and asymmetric when $n_0 \neq n_2$. For waveguiding, the following criteria must be met

$$n_1 > n_0, n_2 \quad (1)$$

There are two different types of electromagnetic modes in dielectric waveguides; they are called guided modes and radiation modes. Figure 5 distinguishes between these two different types of modes. To obtain total internal reflection, the incident angle θ_1 must be greater than the critical angle, θ_c , for each interface. For interface 0,1

$$\theta_1 > \theta_c = \sin^{-1}\left(\frac{n_0}{n_1}\right) \quad (2)$$

For interface 1,2

$$\theta_1 > \theta_c = \sin^{-1}\left(\frac{n_2}{n_1}\right) \quad (3)$$

In Figure 5(a) the light passes through the boundary into the waveguide and through to the next boundary; this is called a radiation mode. Figure 5(b) shows another radiation, or substrate, mode where the light is incident at an angle larger than θ_c for the upper boundary but smaller than θ_c for the lower boundary with n_2 being greater than n_0 . In Figure 5(c) the angle θ_1 surpasses both critical angles of each interface, which results in total internal reflection. Thus, in the guided mode the light is trapped in the guide.

For guided modes¹⁵ and for a certain waveguide thickness, d , and indices n_0 , n_1 , and n_2 , light will propagate in the guide with an angle of incidence θ only if, after two successive reflections, the wave front is again in phase with the original wave front. If this were not the case, after many reflections, somewhere down the waveguide, wave fronts with a range of phases between 0 and 2π would add to zero amplitude, which implies the wave would not propagate. This results in the requirement that at an arbitrary point the phase of one wave front obtained from another by two successive reflections must equal the phase of the second wave front at the same point, or must differ by a multiple of 2π . This requirement permits propagation for only discrete values

¹⁵ Andrews, R. A. "Optical Waveguides and Integrated Optics Technology," Naval Research Laboratory Report 7291 (August 1971).

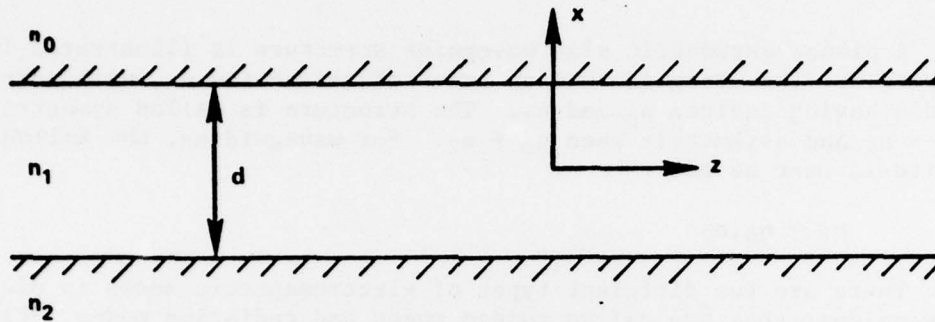


FIGURE 4. Planar Asymmetric Slab Waveguide Structure of Waveguide Thickness d .

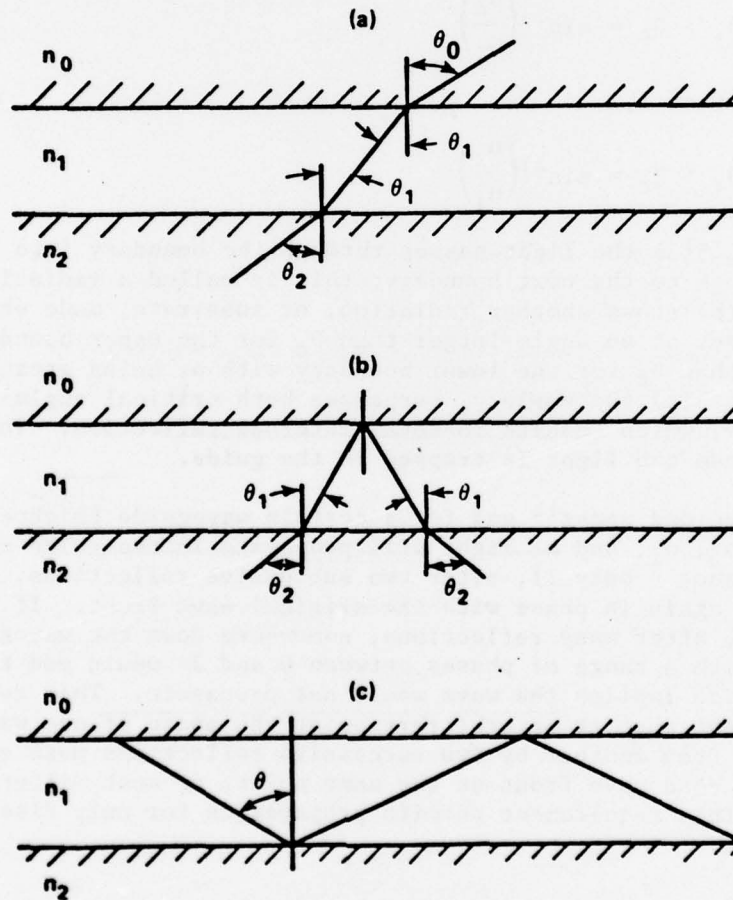


FIGURE 5. Ray Diagrams Illustrating (a) Radiation Modes, (b) Substrate (Radiation) Modes, and (c) Guided Modes.

of θ . Each value of θ is associated with a mode of propagation and each mode has a characteristic velocity of propagation. The velocity of propagation increases as θ increases.

The modes within the waveguide are represented by plane waves traveling in a zigzag path. The modal fields have a propagation constant of k in the direction of travel of the plane wave with β and h being the propagation constants in the z and x directions respectively. Using the coordinate system shown in Figure 4, the fields propagate like $\exp(-i\beta z)$ in the z direction with the propagation constant related to the zigzag angle θ by

$$\beta = kn_1 \sin \theta \quad (4)$$

where $k = 2\pi/\lambda = \omega/c$; λ is the free-space wavelength, ω is the angular frequency of the light, and c is the velocity of light. The critical angle and Eq. 4 give bounds for β , which are

$$kn_1 > \beta > kn_2 \quad (5)$$

The critical angle dictates the upper bound while the lower bound is reached at cutoff. The first three modes are shown in the ω versus β diagram in Figure 6, which indicates the variation of β with frequency ω . Typically, there exists a discrete spectrum of guided modes and a continuous spectrum of radiation modes. The electric field intensity patterns for the three lowest order modes are shown in Figure 7.

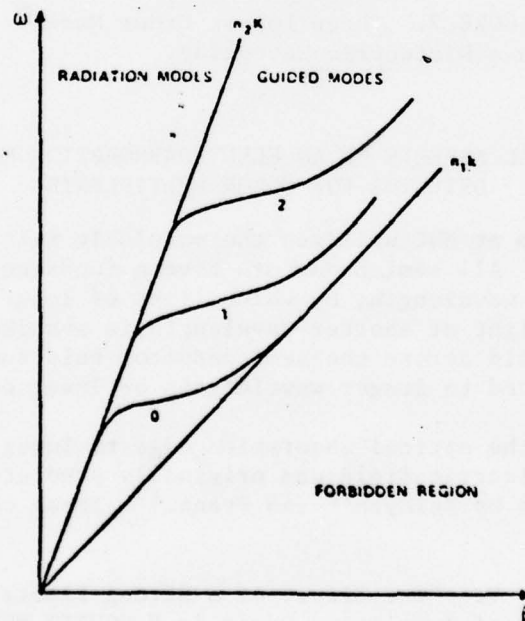


FIGURE 6. Typical ω Versus β Diagram for Three Discrete Guided Modes for Dielectric Slab Waveguides.

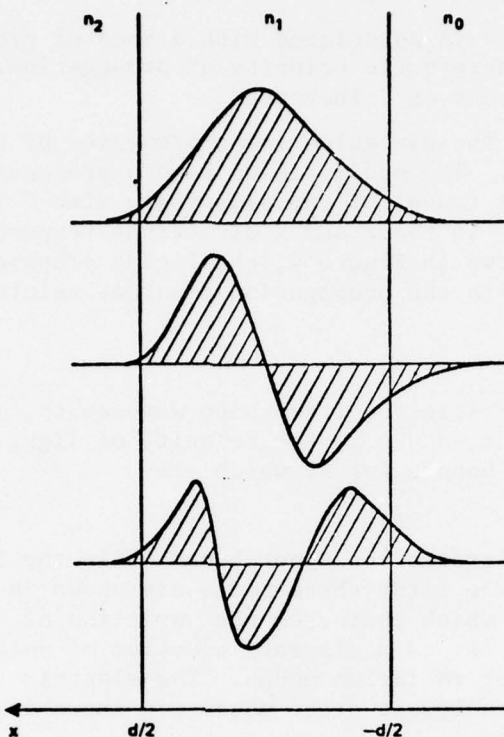


FIGURE 7. Three Lowest Order Modes in a Dielectric Waveguide.

ANALYTICAL ASPECTS OF AN ELECTROABSORPTION MODULATOR/ DETECTOR FOR COLOR MULTIPLEXING

The IO program at NWC utilizes the modulable filter expertise developed at NWC. All semiconductors have a fundamental optical absorption edge at some wavelength, by which light of longer wavelength is transmitted and light of shorter wavelength is absorbed. By applying a large electric field across the semiconductor this fundamental absorption edge is shifted to longer wavelengths or lower energies.

The shift of the optical absorption edge to lower energies under the influence of an electric field was originally predicted for insulators and semiconductors by Keldysh¹⁶ and Franz.¹⁷ These calculations

¹⁶ Keldysh, L. V. "The Effect of a Strong Electric Field on the Optical Properties of Insulating Crystals," SOVIET PHYS JETP, Vol. 34 (November 1958), pp. 788-90.

¹⁷ Franz, W. "Einfluss eines elektrischen Feldes auf eine optische Absorptionskante," Z NATURFORSCH, Vol. 13 (March 1958), pp. 484-89.

together with the experimental observations of this predicted effect by Williams,¹⁸ Moss,¹⁹ Böer and others,²⁰ and Vavilov and Britsyn²¹ opened up a new branch of physics which has since grown and ramified.^{22,23}

The potential use of the Franz-Keldysh effect as a mechanism for intensity light modulation has also been recognized by the early workers in the field,²⁴⁻²⁶ but the nonlinearity of the effect coupled with material difficulties limited the use of these devices.

Recent development in material technology along with the fast growing field of IO has brought about a new look at this mechanism and attempts to devise new electroabsorption (EA) light modulators, switches, and detectors.²⁷⁻³⁰ In many of these applications (excluding modulators) the nonlinearity of this mechanism is of little consequence.

¹⁸ Williams, R. "Electric Field Induced Light Absorption in CdS," PHYS REV, Vol. 117 (March 1960), pp. 1487-90.

¹⁹ Moss, T. S. "Optical Absorption Edge in GaAs and Its Dependence on Electric Field," J APPL PHYS, Vol. 32 (October 1961), pp. 2136-39.

²⁰ Böer, K. W., H. J. Häsche, and U. Kümmel. "Anwendung elektro-optischer Effekte zur Analyse des elektrischen Leitungsvorganges in CdS-Einkristallen," Z PHYS, Vol. 155 (February 1959), pp. 170-83.

²¹ Vavilov, V. S., and K. I. Britsyn. "The Effect of a Strong Electric Field on the Absorption of Light by Silicon," FIZ TVERD TELA, Vol. 2 (August 1960), pp. 1937-39.

²² Cardona, M. *Solid State Physics, Suppl*, Vol. 11, ed. by F. Seitz, D. Turnbull, and H. Ehrenreich. New York, Academic Press, 1969.

²³ *Semiconductors and Semimetals*, Vol. 9, ed. by R. K. Willardson and A. C. Beer. New York, Academic Press, 1972.

²⁴ Eden, R. C., and P. D. Coleman. "Proposal for Microwave Modulation of Light Employing the Shift of Optical Absorption Edge with Applied Electric Field," PROC IEEE, Vol. 51 (December 1963), pp. 1776-77.

²⁵ Racette, G. "Absorption Edge Modulator Utilizing a P-N Junction," PROC IEEE, Vol. 52 (June 1964), p. 716.

²⁶ Handler, P. "Optical Properties of Space-Charge Regions," PHYS REV, Vol. 137A (March 1965), pp. 1862-68.

²⁷ Reinhart, F. K. "Electroabsorption in $\text{Al}_y\text{Ga}_{1-y}\text{As}-\text{Al}_x\text{Ga}_{1-x}\text{As}$ Double Heterostructures," APPL PHYS LETT, Vol. 22 (April 1973), pp. 372-74.

²⁸ Reinhart, F. K., and R. A. Logan. "Monolithic Integrated Coupling of an $\text{Al}_x\text{Ga}_{1-x}\text{As}$ Laser to a Low Loss Passive $\text{Al}_y\text{Ga}_{1-y}\text{As}$ Waveguide." Device Research Conference, Santa Barbara, Calif., March 1974 (unpublished).

²⁹ Dymant, J. C., F. P. Kapron, and A. J. SpringThorpe. "Characterization of Electroabsorption Modulation in Reverse Biased GaAlAs Double Heterostructures." Device Research Conference, Santa Barbara, Calif., March 1974 (unpublished).

³⁰ Stillman, G. E., and others. "Electroabsorption Avalanche Photodiode Detectors." Device Research Conference, Santa Barbara, Calif., March 1974 (unpublished).

Attention is focused in this section on the Franz-Keldysh mechanism in materials as they apply to EA light modulators and detectors. Although the EA formalism is general, the calculations for the EA light attenuation is done for GaAs for wavelengths near $0.9 \mu\text{m}$. The particular device geometry consists of a liquid-phase epitaxy GaAs double heterostructure, as shown in Figure 8. The active region in Figure 8 is n-type rather than the usual p-type GaAs in order to permit electrical isolation in an integrated design.²⁹ Depending upon the application, light is either coupled parallel to the junction (if it is to be used as a component in IO) or transmitted perpendicular to it (GaAs substrate and top electrode can be removed by etching). In both cases, by applying a reverse bias to the device the high electric field within the GaAs material will induce a shift of its optical absorption edge, of gap E_g , to lower energies (the Franz-Keldysh effect). Light of photon energy $\hbar\omega_0 < E_g$ (but near E_g) (see Figure 9) will now be attenuated in passing the GaAs region; electron-hole pairs will be created and swept out to the contacts in the presence of the high electric field (photodetection). Thus, a train of light pulses $\hbar\omega_0$ can be either transmitted for no electric field within the active region or attenuated (modulated/detected) with an applied reverse bias. The prime objective is to determine the optimum conditions for EA light attenuation for various physical parameters of the material and relate them to a particular device application.

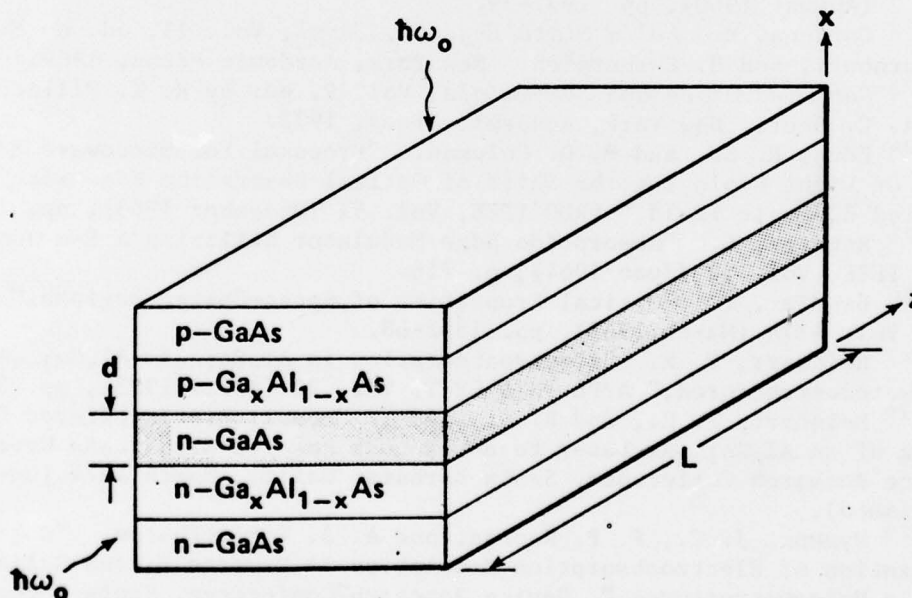


FIGURE 8. GaAs Double-Heterojunction Structure of Length L Used as Electroabsorption Modulator or Detector.

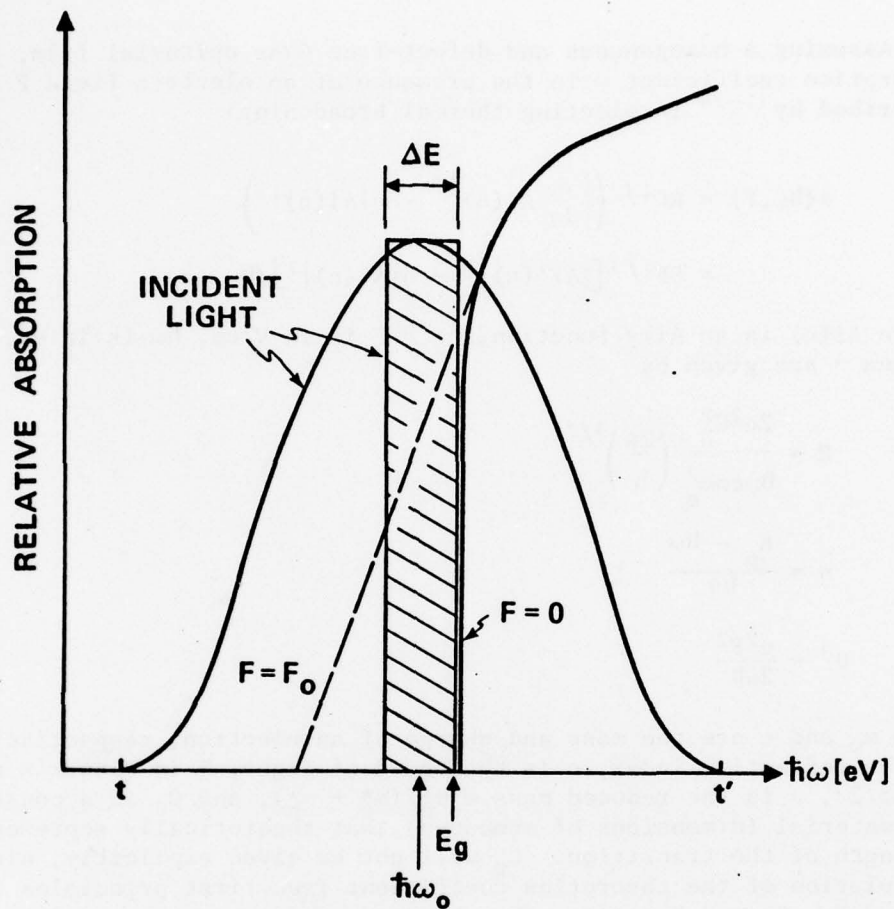


FIGURE 9. Absorption Edge of Waveguide Material for Field-On and Field-Off Conditions as a Function of Photon Energy $\hbar\omega$. E_g is the fundamental gap energy of the material. ω_0 represents the center frequency of the incident light having either a narrow spectral bandwidth ΔE or a spreading $t' - t$.

Assuming a homogeneous and defect-free GaAs epitaxial film, the absorption coefficient α in the presence of an electric field F can be described by³¹⁻³⁴ (neglecting thermal broadening)

$$\begin{aligned}\alpha(\hbar\omega, F) &= R\theta^{1/2} \left(\left| \frac{d}{d\eta} \text{Ai}(\eta) \right|^2 - \eta |\text{Ai}(\eta)|^2 \right) \\ &= \xi F^{1/3} [|\text{Ai}'(\eta)|^2 - \eta |\text{Ai}(\eta)|^2] / \hbar\omega\end{aligned}\quad (6)$$

where $\text{Ai}(\eta)$ is an Airy function,^{31,35} F is in V/cm, $\hbar\omega$ is in eV, and R , η , and θ are given by

$$R = \frac{2e^2 C_0^2}{\hbar\omega c n m_e^2} \left(\frac{2\mu}{\hbar} \right)^{3/2} \quad (7)$$

$$\eta = \frac{E_g - \hbar\omega}{\hbar\theta} \quad (8)$$

$$\theta^3 = \frac{e^2 F^2}{2\mu\hbar} \quad (9)$$

Here m_e and e are the mass and charge of an electron, respectively; n is the refractive index, c is the speed of light, \hbar is Planck's constant/ 2π , μ is the reduced mass $m_e^* m_h^* / (m_e^* + m_h^*)$, and C_0 is a constant of the material (dimensions of momentum) that theoretically represents the strength of the transition. C_0 will not be given explicitly, since no calculation of the absorption coefficient from first principles is intended. C_0 and E_g will rather be used as free parameters in order to fit the limiting case of Eq. 6 for $F \rightarrow 0$ to measured values of the absorption coefficient. For $F \rightarrow 0$, Eq. 6 becomes the familiar expression for the absorption coefficient due to direct allowed transitions behind the edge^{31,33,36} ($\hbar\omega > E_g$)

³¹ Tharmalingam, K. "Optical Absorption in the Presence of a Uniform Field," *PHYS REV*, Vol. 130 (June 1963), pp. 2204-06.

³² Aspnes, D. E. "Electric Field Effects on Optical Absorption Near Threshold in Solids," *PHYS REV*, Vol. 147 (July 1966), pp. 554-66.

³³ Callaway, J. "Optical Absorption in an Electric Field," *PHYS REV*, Vol. 130 (April 1963), pp. 549-53.

³⁴ Callaway, J. "Optical Absorption in an Electric Field," *PHYS REV*, Vol. 134A (May 1964), pp. 998-1000.

³⁵ The Airy function normalization factor used here is the same as that used in the reference cited in Footnote 31, namely, $1/\sqrt{\pi}$.

³⁶ Bardeen, J., F. J. Blatt, and L. A. Hall. *Photography Conference*. New York, Wiley, 1956. P. 146.

$$\alpha(\hbar\omega, 0) = R\pi(\hbar\omega - E_g)^{1/2}/\hbar^{1/2} \quad (10)$$

and gives $\alpha \rightarrow 0$ as $F \rightarrow 0$ in front of the edge ($\hbar\omega < E_g$). C_0 and E_g are adjusted such that Eq. 10 reproduces as close as possible the upper part of the experimental absorption edge. $C_0 = 1.76 \times 10^{12} \text{ cm}^{-1} \text{ sec}^{-1/2}$ and $E_g = 1.42 \text{ eV}$ reproduce the values of Moss¹⁹ for GaAs satisfactorily. Thus, for GaAs, using the reduced mass value of 0.065 m from Moss¹⁹, $\xi = 597.8 \text{ eV (V cm}^2)^{-1/3}$.

Neglecting reflection losses, the transmission of light in an absorbing medium follows Lambert's law:

$$I_t(z) = I_i \exp\left[-\int_0^z \alpha(y) dy\right] \quad (11)$$

where I_i is the incident light intensity and z is the total optical path length traveled. The change in transmitted light intensity given by EA modulation will be

$$\begin{aligned} \Delta I/I &= (I_0 - I_F)/I_0 \\ &= 1 - \exp\left\{-\int_0^z \alpha_F[F(y)] dy + \int_0^z \alpha_0(y) dy\right\} \end{aligned} \quad (12)$$

where the subscript F on α refers to conditions when the electric field is applied and 0 refers to conditions when the field is off. Relations 11 and 12 impose the constraints upon the modulator/detector, which will now be discussed.

For light coupled into the GaAs waveguide (light propagating parallel to the junction), Eq. 11 becomes²⁹

$$I_t/I_i = \left\{ \int S_n(x) \exp[-\alpha(F(x))L] dx \right\} \left[\int S_n(x) dx \right]^{-1} \quad (13)$$

where now α is constant along z but depends upon the electric field in the x direction (see Figure 8). $S_n(x)$ represents the spatial shape of the light intensity of the n th mode within the waveguide. For depletion conditions in the waveguide region, F is linear in x as shown in Figure 10. In this figure F_{s1} is the maximum electric field within the double heterojunction (DHJ) when the depletion depth W is less than the thickness d of the DHJ. For this case

$$F(x) = F_{s1}(1 - x/W) \quad (14)$$

$$\begin{aligned} F_{s1} &= eN_D W / \kappa \epsilon_0 \\ &= [2eN_D(V_D - V_A) / \kappa \epsilon_0]^{1/2} \end{aligned} \quad (15)$$

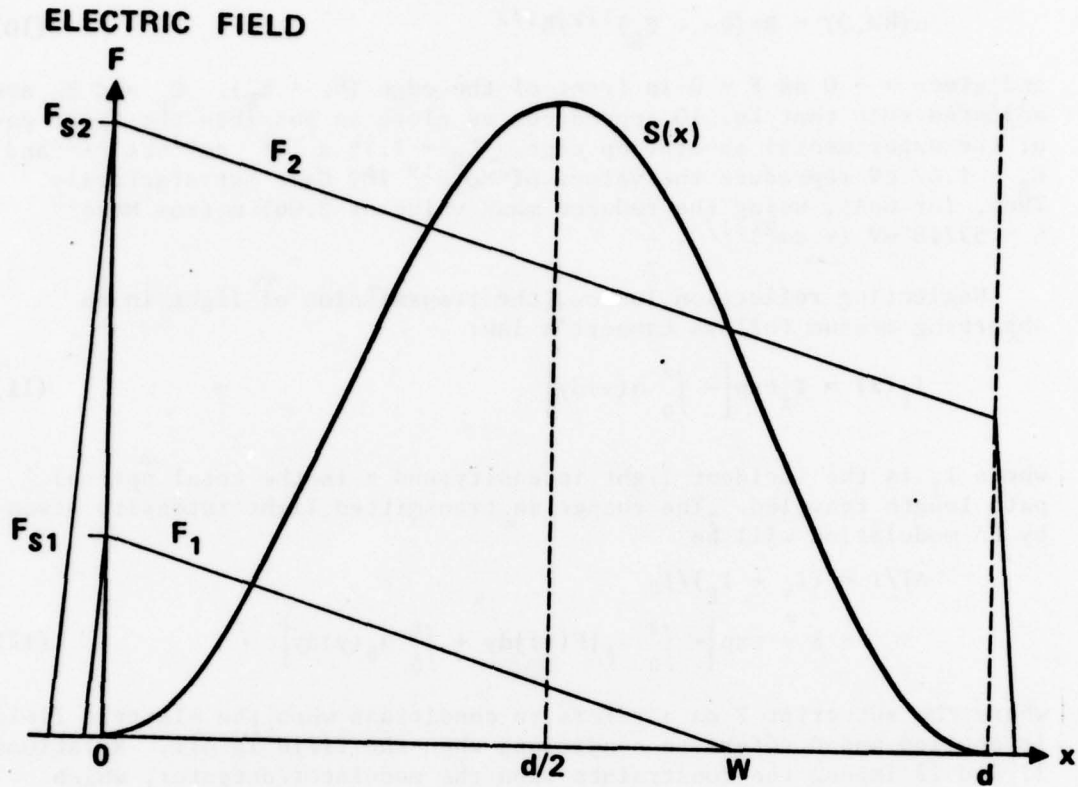


FIGURE 10. Spatial Dependence of Lowest Mode Light Intensity $S(x)$ Within Double-Heterojunction Waveguide of Width d . Superimposed are two electric field profiles (F_1, F_2) under depletion conditions: F_1 , whose depletion depth W falls within the waveguide, and F_2 with W outside the waveguide. F_s represents the maximum electric field at the abrupt junction.

where N_D is the net donor concentration, κ is the static dielectric constant of the junction material, ϵ_0 is the permittivity of free space, and $V = V_D - V_A$ is the difference between the applied and the flat-band voltage. When the applied voltage is such that the electric field reaches through the junction ($W > d$),

$$F(x) = F_{s2} (1 - x/d) + V/d - \frac{1}{2} F_{s2} \quad (16)$$

where now F_{s2} is the maximum electric field corresponding to $W = d$ in Eq. 14 [for some voltage $V_1 = V_d - V_A = d^2 e N_D / (2 \kappa \epsilon_0)$].

Assuming $S(x) = \sin^2(x\pi/d)$ for the lowest propagating mode,³⁷ expression 13 now becomes

$$I_t/I_i = (2/d) \int_0^{(d,W)} \sin^2(x\pi/d) \times \exp[-\xi L \{ \text{Airy} \} F(x)^{1/3} / \hbar \omega] dx \quad (17)$$

where L is the waveguide length and $\{ \text{Airy} \}$ is the Airy function in the parentheses in expression 6. The upper limit of integration (whether d or W) and the corresponding expression for $F(x)$ [whether Eq. 14 or Eq. 16] is determined from the condition $d \geq W$ (see Figure 10).

I_t/I_i has been calculated from Eq. 17 as a function of $|V_D - V_A|$ bias under the following conditions: GaAs $E_g = 1.415$ eV at 300°K; incident unpolarized monochromatic light; $d = 10^{-4}$ cm, $L = 0.05$ cm. Light attenuation in decibels for various values of net donor concentrations N_D are shown in Figure 11.

It is to be noted that for these conditions optimum light attenuation, and thus photodetection, occurs for $N_D = 10^{15}/\text{cm}^3$ or less. However, no substantial increase in light attenuation is obtained by reducing the net donor concentration of the active region below $10^{15}/\text{cm}^3$. This follows from relation 16, where for values of N_D lower than $10^{15}/\text{cm}^3$ the electric field is nearly independent of N_D , i.e., the GaAs active region behaves for all practical purposes as an insulator. The reason for the sudden increase in light attenuation below $5 \times 10^{16}/\text{cm}^3$ can be explained by considering the reach-through voltage V_1 in the DHJ. When the bias voltage $|V_D - V_A|$ is less than $|V_1|$ only parts of the light intensity envelope $S(x)$ within the DHJ are affected by the electric field, i.e., the electric field induces light attenuation only at points $x < W$, and the overall light attenuation within the junction will be relatively small. This is the case for $N_D = 5 \times 10^{16}/\text{cm}^3$ in Figure 11, where V_1 is about 41 V. When V_1 is reached, the entire envelope $S(x)$ is affected by the electric field and there will be a drastic increase in light attenuation within the junction (as in the case for $5 \times 10^{15}/\text{cm}^3$ in Figure 11, where V_1 is 4.1 V).

For practical device consideration, DHJs having $N_D \geq 5 \times 10^{16}/\text{cm}^3$ in the active region would require large voltages to achieve reach-through (thus substantial light attenuation); this, in turn, would lead to a high electric field near the junction (for $N_D = 5 \times 10^{16}/\text{cm}^3$, $V_1 = 41$ V, and $F_{s2} = 820$ kV/cm) and thus eventual breakdown of the

³⁷ The boundary conditions were chosen in such a way as to terminate the optical field at the junction interfaces, i.e., the alloy regions were assumed to be perfect conductors.

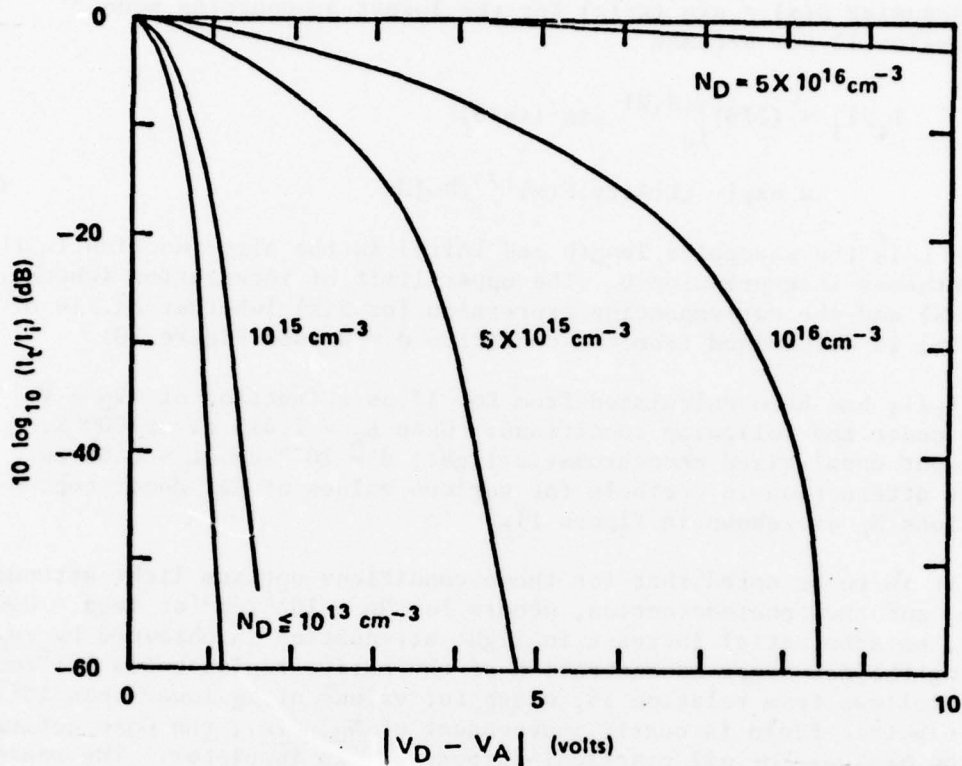


FIGURE 11. Electroabsorption-induced Light Attenuation in Decibels as a Function of Reverse Bias Voltage $|V_D - V_A|$ and Net Donor Concentration N_D When Incident Light of Energy $\hbar\omega_0$ Near Edge is Coupled Into Waveguide (Parallel to Junction). Equation 17 was used in calculating the ratio of the transmitted to incident intensity, I_t/I_i , under the following conditions: GaAs $E_g = 1.415$ eV at 300°K; incident unpolarized monochromatic light of photon energy $(E_g - \hbar\omega_0) = 0.005$ eV; $d = 10^{-4}$ cm; $L = 0.05$ cm; W and F_s were calculated from Eq. 14 and 16.

device. Nothing substantial is gained in terms of light attenuation by making $N_D < 10^{15}/\text{cm}^3$. In the extreme case of semi-insulating (compensated) GaAs film, although high attenuation can be achieved with minimum voltage, the insertion losses of such a material would be prohibitive as will be seen below.

The light attenuation as a function of $|V_D - V_A|$ bias for various photon energies $\hbar\omega$ is shown in Figure 12. Here equal intensities for each $\hbar\omega$ were assumed and the value of N_D was 10^{15} cm^3 .

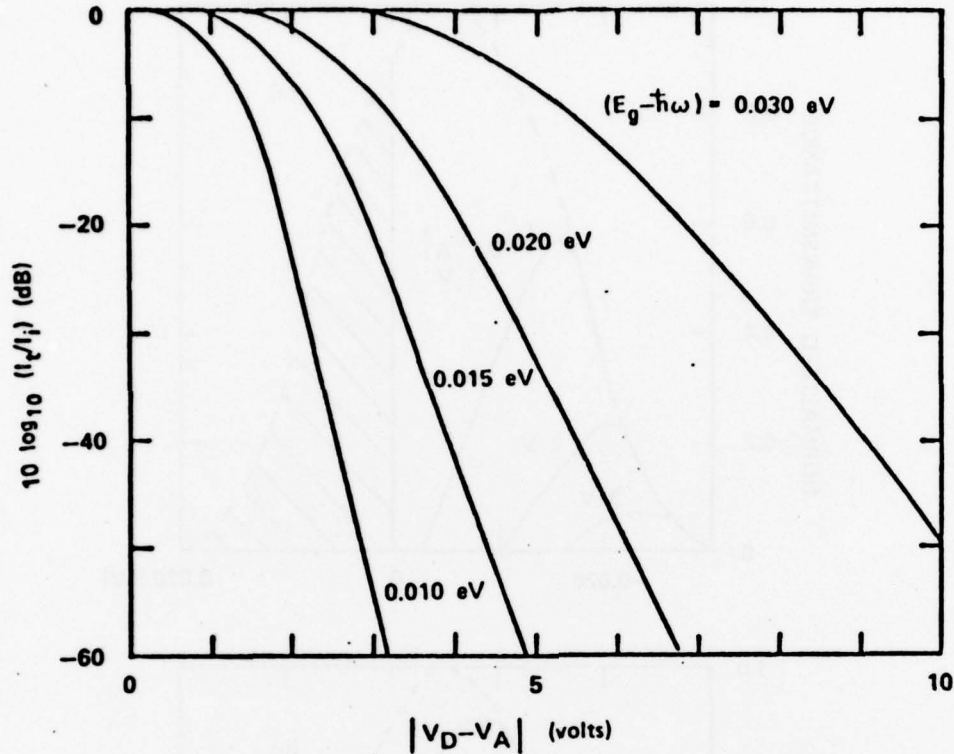


FIGURE 12. Electroabsorption-Induced Light Attenuation in Decibels Calculated From Eq. 17 as a Function of Reverse-Bias Voltage $|V_D - V_A|$ for Various Photon Energies $\hbar\omega$. Value of the net donor concentration N_D was $10^{15}/\text{cm}^3$; the physical parameters of the waveguide were the same as those in Figure 11.

When a broad-band light source is incident on the device there will be a selective attenuation and detection of the incident radiation within a wavelength interval.²⁹ Assuming a $\sin^2[(\hbar\omega - t)\pi/(t' - t)]$ (t has the unit of energy) dependence in the spectral energy of the incident light (say an LED source) shown in Figure 9, we get the relative transmittance shown in Figure 13 for various values of applied reverse bias. Figure 13 indicates that more than one channel of information can be utilized from a common source. Two junctions modulated by an AC voltage superimposed on different DC bias voltages will result in modulation of different spectral information through the waveguide. Furthermore, if two similar devices were in series and biased appropriately the first would absorb and thus detect its associated channel of information, and pass the second spectral band to the other detector.

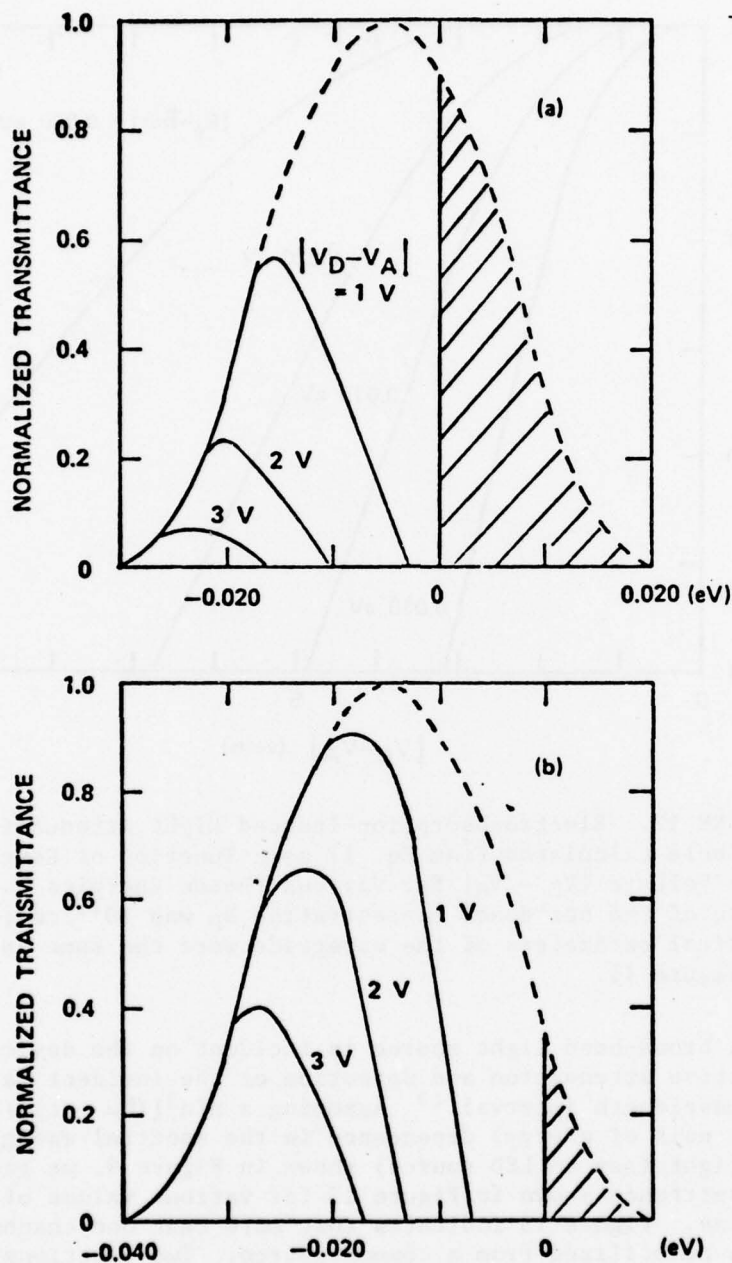


FIGURE 13. Relative Transmittance Through GaAs Waveguide for LED Light Source (Shown by Dotted Lines) for Various Values of Reverse-bias Voltage $|V_D - V_A|$. ω_0 is the center frequency of the source for (a) $E_g - \hbar\omega_0 = 0.005$ eV and (b) $E_g - \hbar\omega_0 = 0.015$ eV. The shaded region indicates the overlap of the incident radiation and the absorption edge of the material with gap E_g .

The insertion losses within the GaAs waveguide are critical due to the nature of this geometry, $d \ll L$; i.e., the light path length will be much longer than the wavelength of light. Consequently, a loss of 10% will occur even with relatively pure GaAs films, say $\alpha_0 = 10/\text{cm}$ at the desired wavelength. Semi-insulating GaAs or any other film having impurities and inhomogeneities would broaden considerably the zero-field absorption edge α_0 ,³⁸⁻⁴² making it almost useless as a modulator of light.

These analytical results emphasize the doping levels and geometry needed to optimize an EA light modulator and detector. Optimum transmission and EA attenuation of radiation through a DHJ waveguide will occur for net donor concentrations of $10^{15}/\text{cm}^3$ or less; such waveguides must be homogeneous and defect-free to reduce the insertion losses for zero electric field. The above applies to a GaAs compound or one of its alloys (Ga-As-Sb or Ga-Al-As), although with present double-heterostructure technology it is uncertain how sharp the absorption edge can be made for these alloys. Theoretically, EA light attenuation of 20 dB or larger can be achieved in DHJ waveguides 0.05 cm long with nominal voltages of 0-10 V across a 1- μm junction for photon energies 0.030 eV below the absorption edge. If a broad-band source is coupled to a waveguide, the waveguide will attenuate and detect different bands of wavelengths for different applied voltages, thus making it useful in color multiplexing schemes.

Placing a relatively small AC voltage superimposed on a DC reverse bias across the junction of a GaAs heterostructure diode allows wavelength selective amplitude modulation in various spectral regions of a white light beam. If two similar diodes are operated in parallel as shown in Figure 14, then two well-separated channels of information can be imposed on the same LED. By using two diodes similar to the modulating diodes but connected in series, one may independently absorb and detect the modulations and read them out as junction photocurrent as

³⁸ Lambert, L. M. "Optical Absorption in an Electric Field in Semi-Insulating Gallium Arsenide," J PHYS CHEM SOLIDS, Vol. 26 (September 1965), pp. 1409-18.

³⁹ Redfield, D. "Electric Fields of Defects in Solids," PHYS REV, Vol. 130 (May 1963), pp. 914-15.

⁴⁰ Redfield, D. "Effect of Defect Fields on the Optical Absorption Edge," PHYS REV, Vol. 130 (May 1963), pp. 915-18.

⁴¹ Redfield, D., and M. A. Fromowitz. "The Direct Absorption Edge in Covalent Solids," APPL PHYS LETT, Vol. 11 (August 1967), pp. 138-40.

⁴² Redfield, D. "Effect of Charged Surfaces on the Optical Absorption Edge," PHYS REV, Vol. 140A (December 1965), pp. 2056-58.

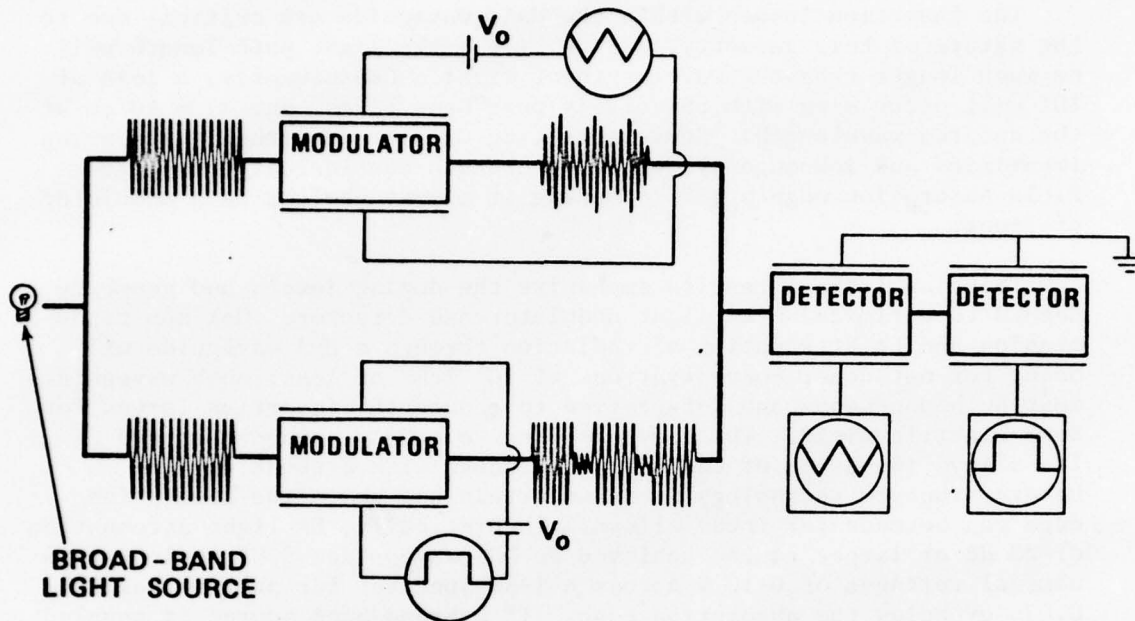


FIGURE 14. Two-Channel Color Multiplexer and Demodulator.

shown in Figure 14. Therefore, by monitoring the current, this device can be used to deduce the intensity of radiation absorbed by the diode. Depending on the wavelengths to be detected and how the detector electronics are designed, either the LED radiation is absorbed within the junction or the radiation passes through the junction unaffected. The second diode in series will then absorb, thus detect, the second channel of information.

If the spectral characteristics of the light source are as shown in Figure 13, several channels of information can be imposed on the beam. Depending upon the energy location of the absorption edge of the diodes with respect to the energy distribution of the LED, a different number of channels are accessible as the two cases in Figure 13 indicate. The first case provides for a few channels and a smaller energy separation between channels. An advantage of the second case is that not only is there a larger separation between channels but also each channel contains more intensity than the previous case. The detectors would be placed at some distant point from the modulators. Of course the proper channel of information would have to be modulated into the appropriate wavelength spectrum such that the correct detector is able to detect the information. For example, if two channels are to be modulated and detected simultaneously, the information to be detected by the first detector must be at a longer wavelength than that of the second detector.

A family of transmission curves plotted versus wavelength⁴³ where each curve represents a different electric field, F , across the GaAs is plotted in Figure 15. If the field across the semiconductor, GaAs, is varied from 40,000 to 70,000 V/cm then the transmission of light at 8,500 Å varies from 20% to less than 1%. At 8,550 Å transmission varies from 45 to 8%, while at 8,600 Å transmission varies from 48 to 23%. One must keep in mind that there is a 50% reflection loss at the first interface; this is why the values are so low. Light at wavelengths longer than 8,650 Å is passed relatively unaffected by the modulator, while light at wavelengths shorter than 8,400 Å is totally absorbed by the modulator. If one assumes that the light incident on the modulator has uniform spectral intensity and passes the modulated output into a detector with flat spectral response out to 8,600 Å and zero response beyond that, then one should observe a maximum detector voltage proportional to the sum of the absorptions at the different wavelengths at 40,000 V/cm and a minimum detector voltage proportional to the sum of the absorptions at the different wavelengths at 70,000 V/cm. Therefore, the informational content at a given wavelength, λ_0 , for a modulator operated between two electric field extremes, F_1 and F_2 , is just proportional to $\tau(F_1, \lambda_0) - \tau(F_2, \lambda_0)$ or $\Delta\tau$, the difference between the transmissions at F_1 and F_2 . Figure 16 shows a plot of $\Delta\tau$ versus λ for $F_1 = 20,000$ V/cm and $F_2 = 40,000$ V/cm in GaAs taken from the data in Figure 15. Changing the DC bias field $(F_1 + F_2)/2$, simply shifts λ_m , the wavelength at which the maximum in $\Delta\tau$ occurs. In GaAs, λ_m increases about 1 Å for an increase in reverse bias of 350 V/cm (although the position of λ_m is not quite linear with increasing field).

The next thing to consider is the effects of a temperature variation. When the temperature of the modulator increases, two things happen. First, the band-gap energy decreases and therefore λ_m increases, because it is inversely proportional to the band-gap energy. For GaAs at about room temperature this increase is about 2.6 Å/°K. Second, the knee in the transmission curve (of Figure 15) near maximum transmission gets somewhat less sharp as temperature rises, which tends to broaden the band of wavelengths over which modulation is imposed by each of the modulators. If there is a temperature fluctuation of $\pm 30^\circ\text{K}$, which corresponds to about 156 Å of fluctuation of λ_m (the peak modulation), and a maximum electric field of 70,000 V/cm, which corresponds to a 200-Å shift of this peak, it becomes difficult to achieve a two-channel system without cross talk between the two channels. If temperature changes of this magnitude are to be considered, and they need to be if this system is to be used on an aircraft or ship, some sort of temperature compensation needs to be implemented. One method is to alloy the junction

⁴³ Naval Weapons Center. *Modulable Filters: Concepts and Parameters*, by N. Bottka and V. Rehn. China Lake, Calif., NWC, January 1974. (NWC TN 601-1).

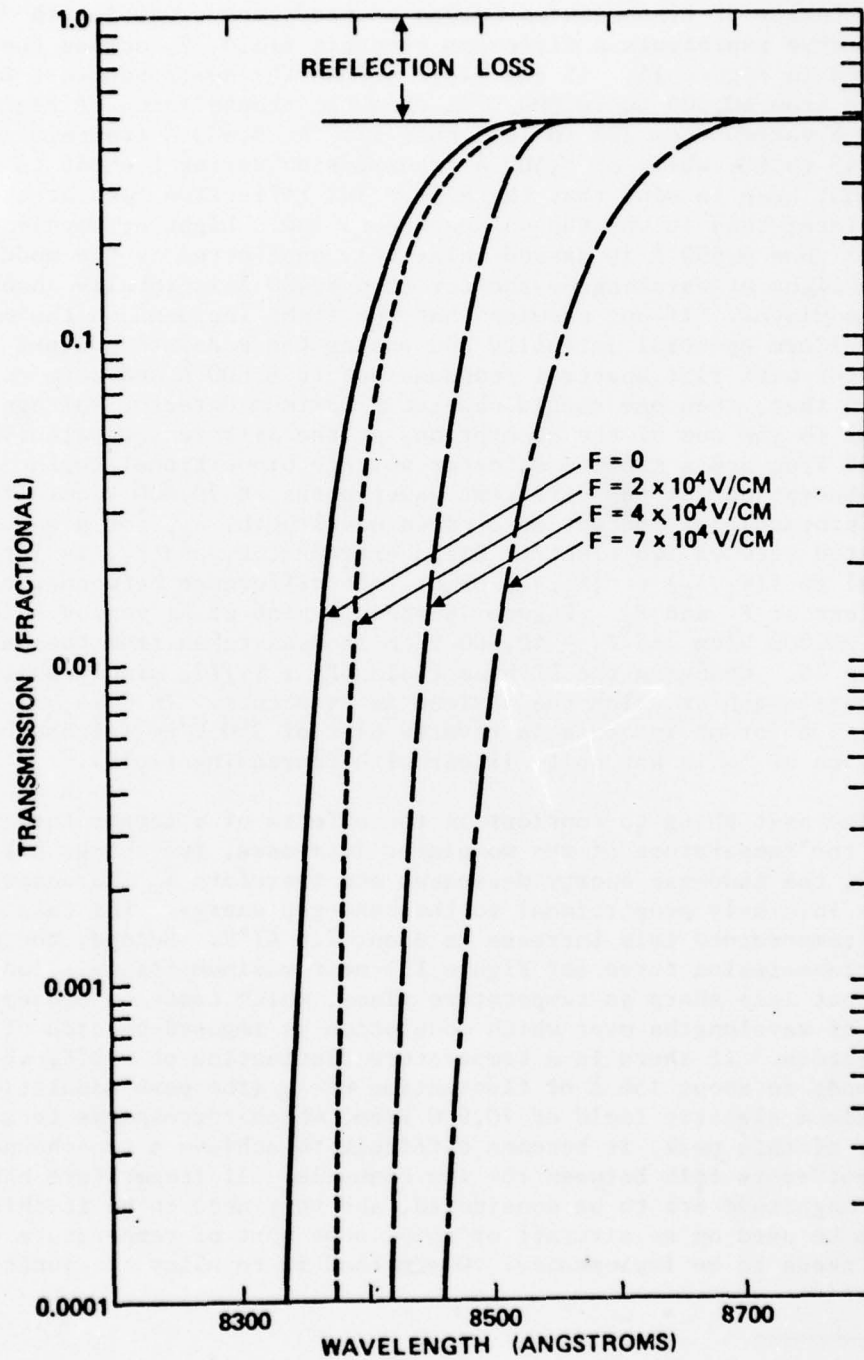


FIGURE 15. Transmission Versus Wavelength for Several Electric Field Strengths in GaAs.

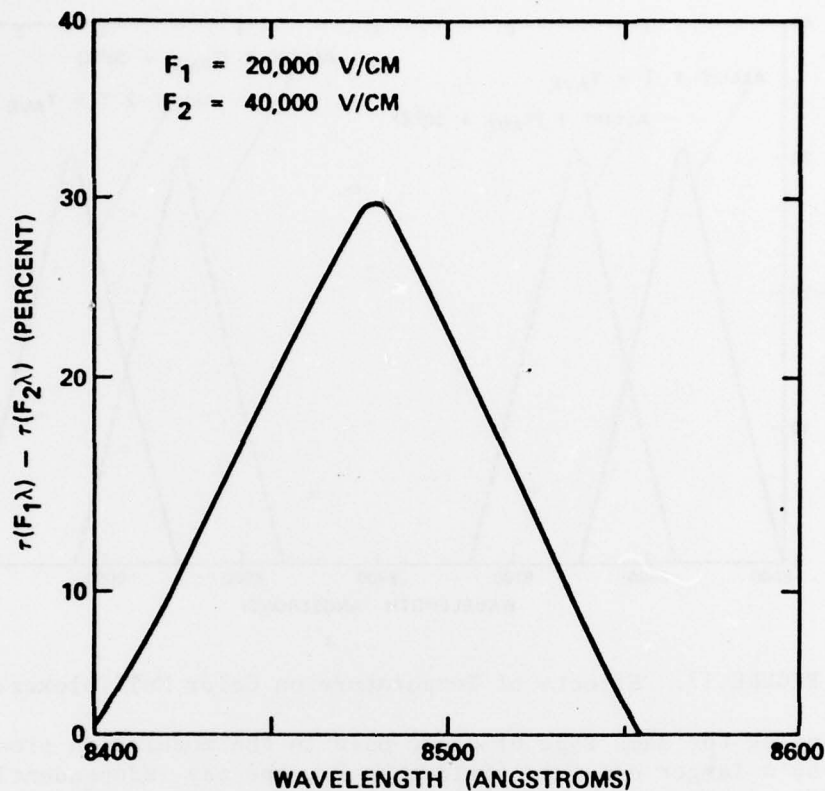


FIGURE 16. Modulation Versus Wavelength of Franz-Keldysh Junction Modulator.

region of the modulator and detector. A continuous system of alloys¹⁴ $\text{Ga}_{1-x}\text{Al}_x\text{As}$ exists in which the room temperature λ_m varies from about 9,000 Å to about 8,500 Å as x goes from 0 to 0.07. Also, it has been shown that $\text{Ga}_{1-x}\text{Al}_x\text{As}$ alloyed diodes with various concentrations can be grown epitaxially on the same substrate.²⁹ Therefore, with 500 Å of available modulation range and only 156 Å of temperature fluctuation it is obvious that there is available bandwidth for two channels. Figure 17 depicts the modulation versus wavelength at two discrete wavelengths produced by two differently alloyed diodes operated between the same electric field limits $F_1 \cdot F_2$. Replotting the curves for different temperatures, where the shorter wavelength peak is shifted to longer wavelengths by a 30°K higher temperature and the longer wavelength peak is shifted to a shorter by a 30°K lower temperature, shows that the 60°K temperature spread causes no observable mixing of the two channels.

¹⁴ Kressel, H., and others. "Heterojunction Laser Diodes for Room Temperature Operation," OPT ENG, Vol. 13 (September 1974), pp. 416-22.

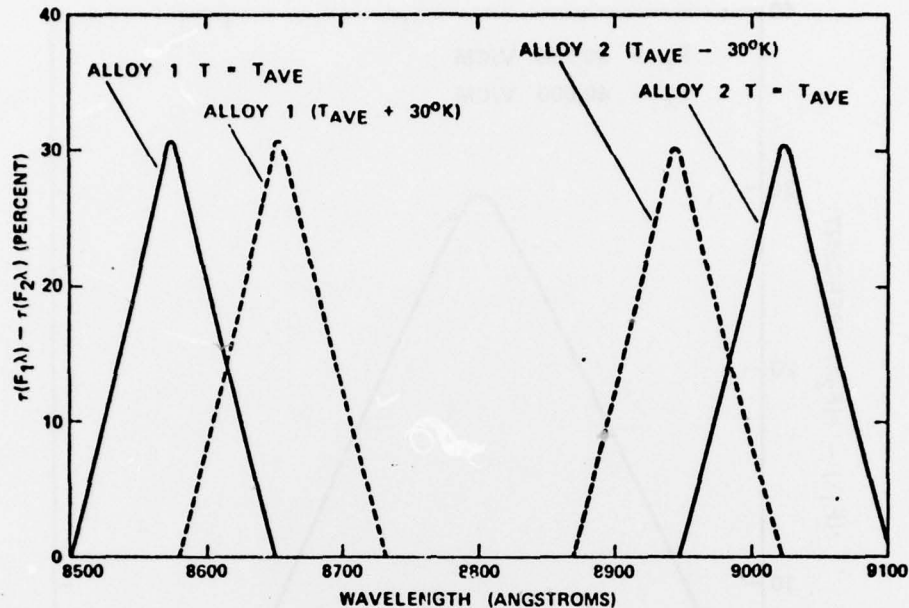


FIGURE 17. Effects of Temperature on Color Multiplexer.

By using the same type of diode used in the modulation process but biased by a larger electric field than F_2 , one may independently detect the short wavelength channel, which is then all absorbed out of the beam. By applying an even larger field to another downstream detector one may absorb and detect the longer wavelength channel of information. However, optimum positioning of the detector's absorption cutoff wavelength using only electric fields is impossible because of the large wavelength spread between the two modulation peaks shown in Figure 17. Therefore, for the first channel detector it is necessary to obtain a different alloy, intermediate in composition between the two alloys used for the two modulators. Figure 18 shows the effects of $\pm 30^\circ\text{K}$ temperature changes about the averages for both the modulators and detectors. When the modulator temperatures are shifted $+30^\circ\text{K}$ from their average and the detector temperatures are shifted -30°K from their average, some of the first channel (short wavelength) information is not absorbed out at the first detector and is passed on to the second detector, where it is detected as cross talk. For the curves shown in Figure 18 this amounts to about 10% of the total first channel information for the aforementioned worst case temperature shift. Similarly, when the modulator substrate temperature is lowered by 30°K while the detector substrate temperature is raised 30°K , about 10% of the second channel of information shown in Figure 18 is absorbed by the first channel detector. This cross talk may be reduced substantially by choosing modulators with more diverse alloy compositions and thereby increasing the wavelength spread between modulation peaks.

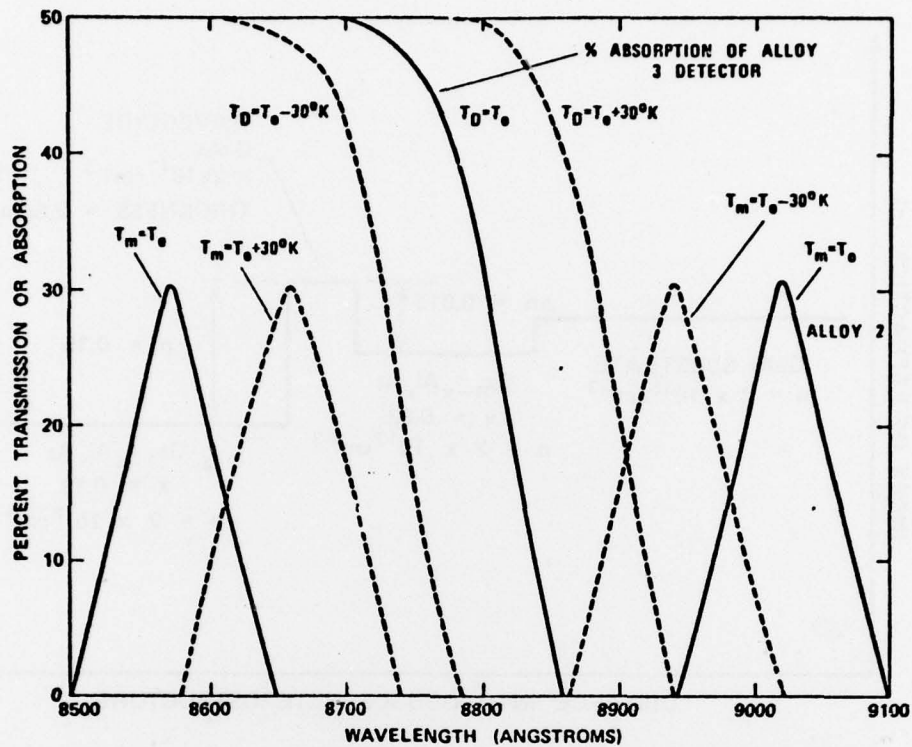


FIGURE 18. Effects of Temperature on Multiplexing and Demodulating System.

EXPERIMENTAL ASPECTS OF THE EA MODULATOR AND DETECTOR

At NWC several GaAlAs double-heterostructure diodes have been tested for modulation purposes. The most promising diode that was obtained has the characteristics shown in Figure 19. A 10-dB attenuation of light was achieved with a 10-V reverse bias. There are two reasons why the diode did not perform as a good modulator. One is that the waveguide thickness was too large (2.5 μm). The waveguide could only be partially depleted with the applied electric field. This means that only a portion of the light intensity distribution over the waveguide was affected by the electric field. The second reason is that the doping density in the active region was also too large ($2 \times 10^{17} \text{ cm}^{-3}$), which requires too large an electric field to deplete the waveguide. This doping density would probably have been adequate if the waveguide thickness had been less than 1 μm . NWC has been trying to obtain suitable materials but has had little success in getting them.

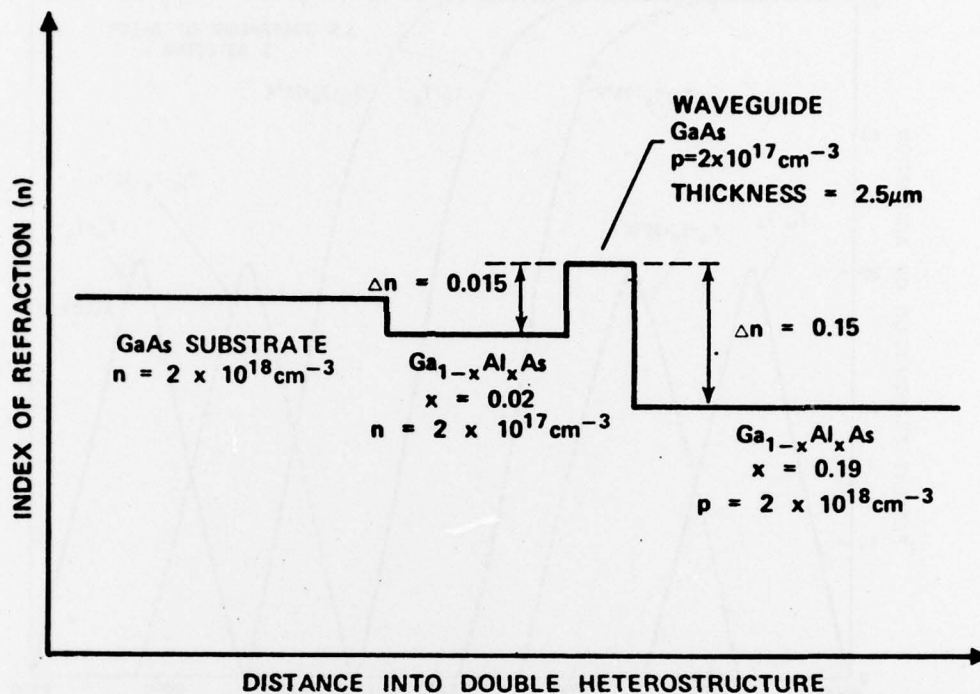


FIGURE 19. Index of Refraction of Various Layers of Double Heterojunction Device Used To Measure Electroabsorption Effect.

Beli-Northern Research Ltd., Ottawa, Canada, has succeeded in growing the materials needed to make good modulators and detectors. The following paragraphs present some of the more important results they have obtained. A more complete discussion of their results is found in the literature.⁴⁵

Figure 20 shows typical attenuation measurements as a function of applied reverse bias for the double heterostructure modulator shown in the inset of Figure 20. The doping density within the waveguide was $1.5 \times 10^{17} \text{ cm}^{-3}$ but the waveguide thickness was only $0.7 \text{ } \mu\text{m}$, which allowed sufficient depletion to achieve large attenuation. The experiment was performed by coupling a $30\text{-}\text{\AA}$ -wide monochromator source into

⁴⁵ Dymont, J. C., F. P. Kapron, and A. J. SpringThorpe. "Devices Based on Electroabsorption (EA) Effects in Reverse-Biased GaAs-GaAlAs Double Heterostructures," in *Proceedings of Fifth International Symposium on GaAs*, Conference Series No. 24. British Institute of Physics, 1975. Pp. 200-209.

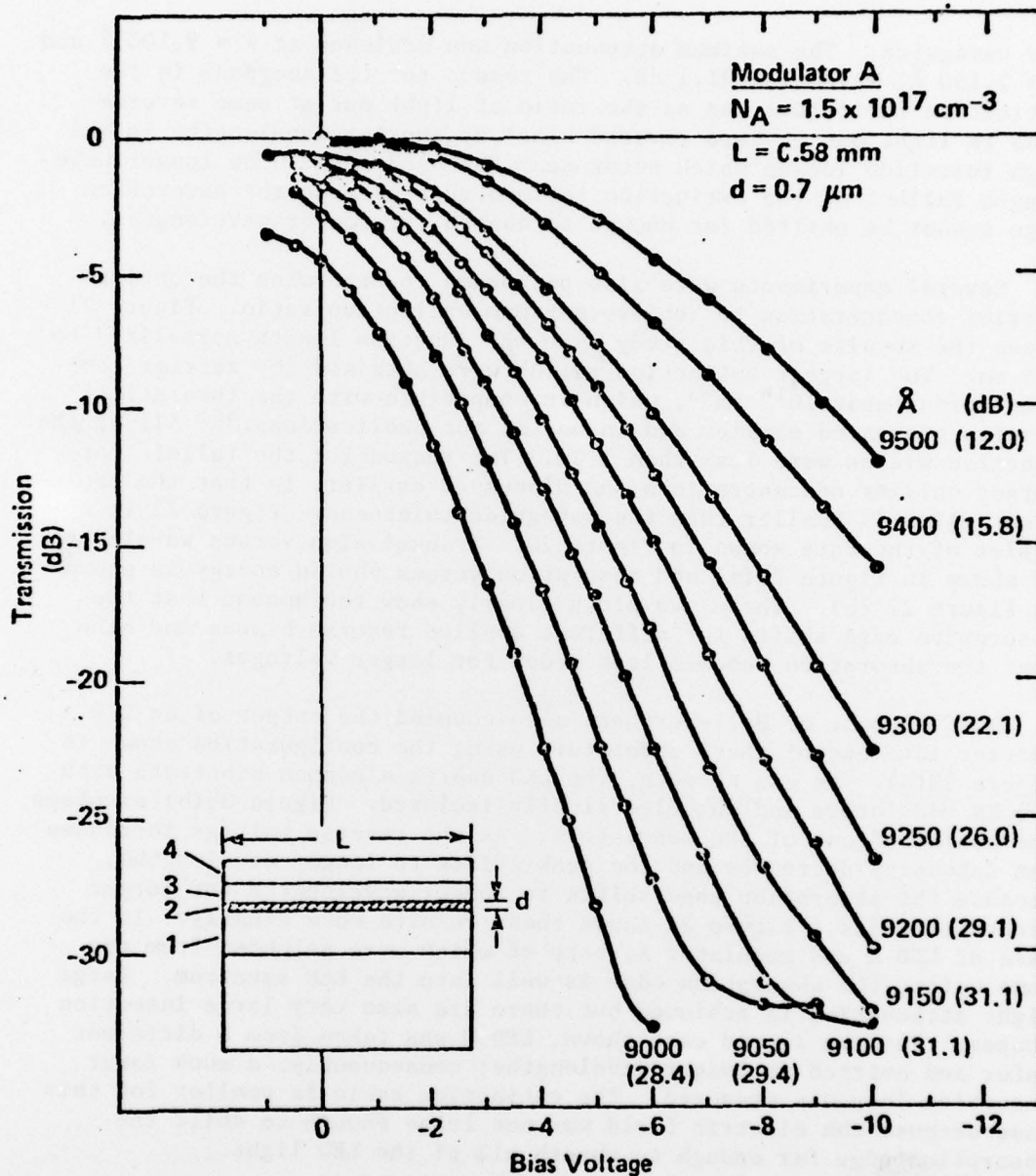


FIGURE 20. Typical Data From Double Heterojunction Modulator (See Inset) of Length 0.58 mm Showing Light Transmission Versus Bias Voltage for Several Wavelengths. Layers 1 and 3 are, respectively, n-type and p-type $\text{Ga}_{1-x}\text{Al}_x\text{As}$ ($x = 0.35$), and layer 4 is p-type GaAs . The higher index guiding layer 2 has thickness d and is either p-type or n-type $\text{Ga}_{1-y}\text{Al}_y\text{As}$ (with y between 0 and 0.10). Numbers in parentheses after each wavelength are extinction ratios. (From reference cited in Footnote 45.)

the waveguide. The maximum attenuation was achieved at $\lambda = 9,100 \text{ \AA}$ and $\lambda = 9,150 \text{ \AA}$, which was 31.1 dB. The reason for the decrease in the extinction ratio (defined as the ratio of light out at some reverse bias to light out at zero reverse bias) at shorter wavelengths is the high insertion losses which occur near the band edge. The longer wavelength falloff of the extinction ratio occurs because the absorption edge cannot be shifted far enough to absorb the longer wavelengths.

Several experiments were also performed to determine the optimum carrier concentration to achieve maximum extinction ratio. Figure 21 shows the results of this study with the junction length normalized to 0.5 mm. The largest extinction ratios were obtained for carrier concentrations near 10^{16} cm^{-3} , which is compatible with the theoretical results presented earlier and in one of our publications.⁴⁶ All of the junction widths were less than 1 μm . The reason for the falloff for larger carrier concentrations, as discussed earlier, is that the depletion region is smaller than the waveguide thickness. Figure 22 is a replot of the data shown in Figure 20. Transmission versus wavelength is shown in Figure 22(a) and absorption versus photon energy is shown in Figure 22 (b). These two plots clearly show the amount that the absorption edge shifts for different applied reverse biases and also that the absorption becomes less steep for larger voltages.

J. C. Dymont of Bell-Northern also coupled the output of an LED emitter into one of these modulators using the configuration shown in Figure 23(a). As can be seen, the LED shares a common substrate with two EA modulators and was electrically isolated. Figure 23(b) displays the output of one of the modulators. As the reverse voltage increases the intensity decreases and the peak shifts to longer wavelengths, because the absorption edge shifts to longer wavelengths for larger electric fields. Figure 24 shows these results more clearly. In the case of LED A and modulator A, both of which were selected from the same wafer, the absorption edge is well into the LED spectrum. Large light attenuation is achieved but there are also very large insertion losses. For the second case shown, LED Q was taken from a different wafer and emitted at longer wavelengths; consequently, a much lower insertion loss was measured. The extinction ratio is smaller for this case because the electric field was not large enough to shift the absorption edge far enough to absorb all of the LED light.

⁴⁶ Bottka, N., and L. D. Hutcheson. "Analytical Aspects of Electro-absorption Modulators," J APPL PHYS, Vol. 46 (June 1975), pp. 2645-49.

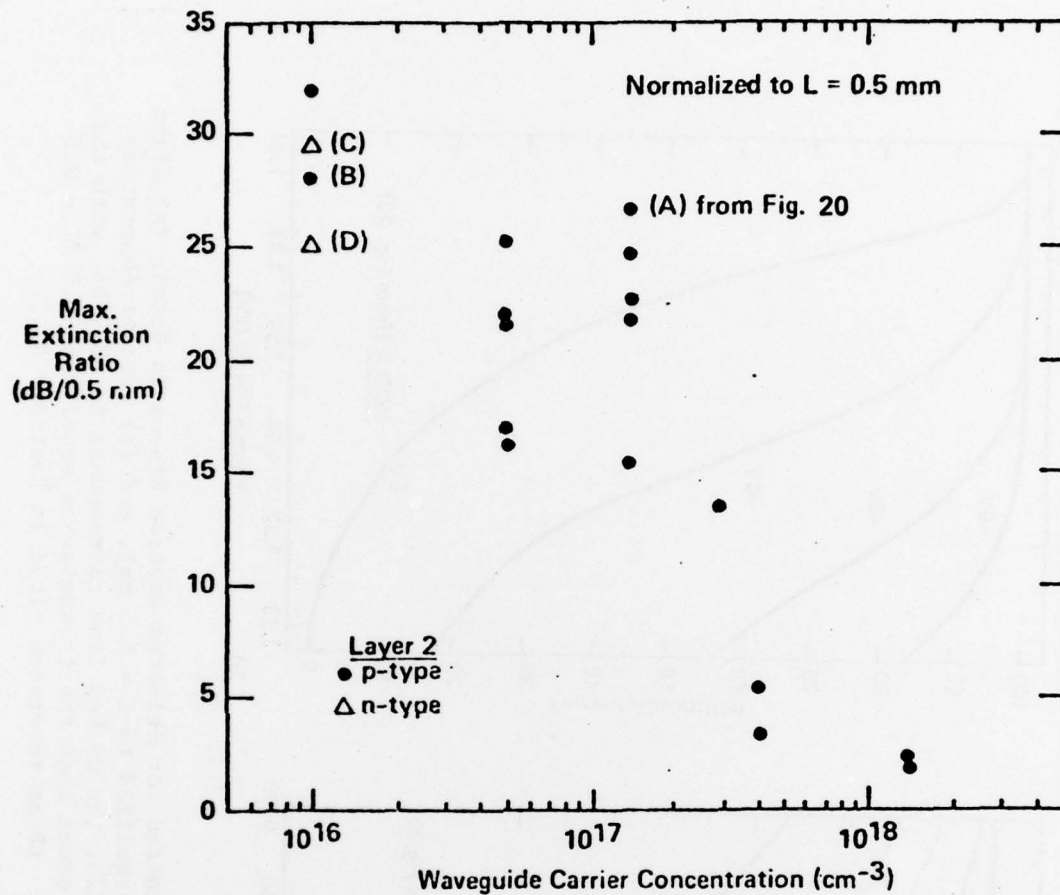


FIGURE 21. Maximum Extinction Ratio as Function of Carrier Concentration in Guiding Layer 2, With Data Normalized to $L = 0.5$ mm. The point labeled A corresponds to the modulator of Figure 20. Three other modulators, B, C, D, are indicated. (From reference cited in Footnote 45.)

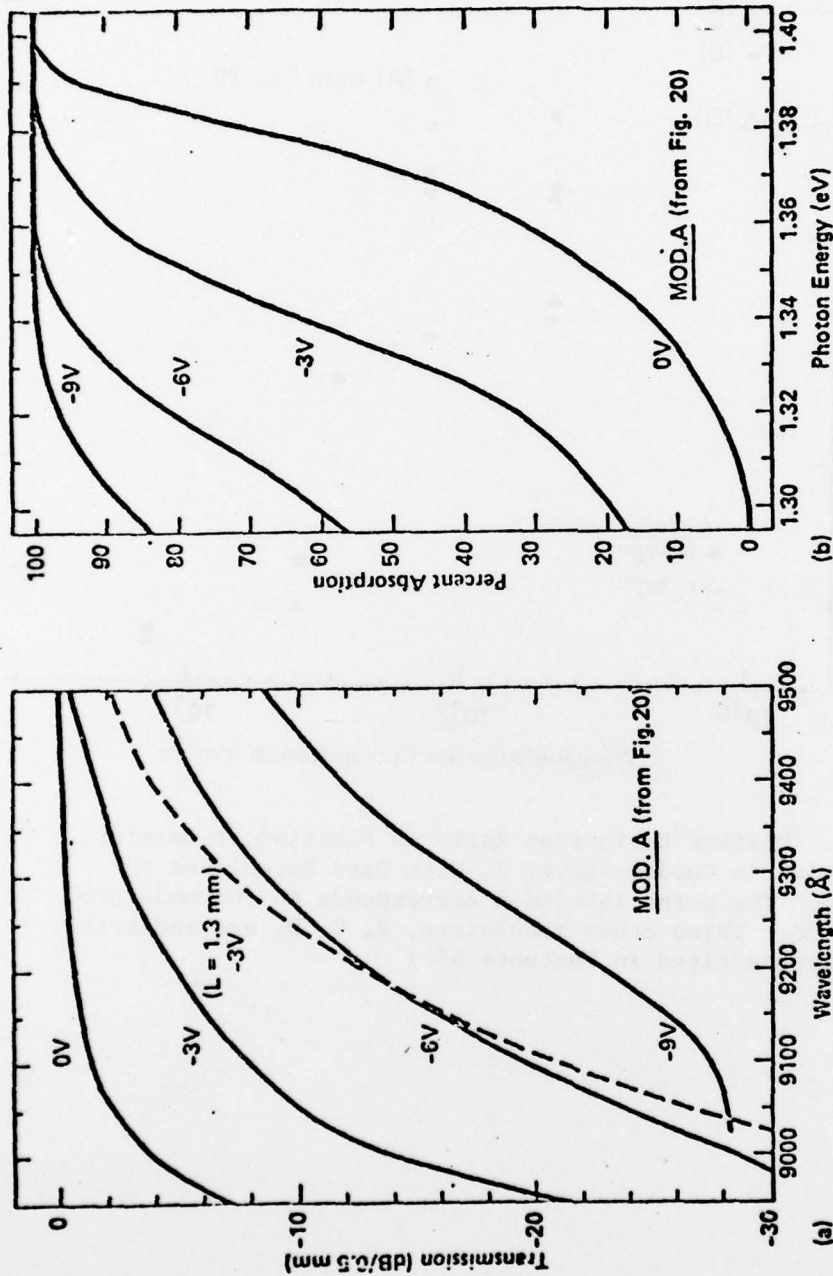


FIGURE 22. Data of Figure 20 Replotted for Selected Reverse Biases To Obtain (a) Light Transmission Versus Wavelength (Normalized to $L = 0.5$ mm), and (b) Percent Absorption Versus Photon Energy. In Figure 22a, the dashed line corresponds to -3 V but with the length increased to $L = 1.3$ mm in order that the transmission equal the -6 V ($L = 0.5$ mm) value of -15 dB at $\lambda = 9170$ Å. (From reference cited in Footnote 45.)

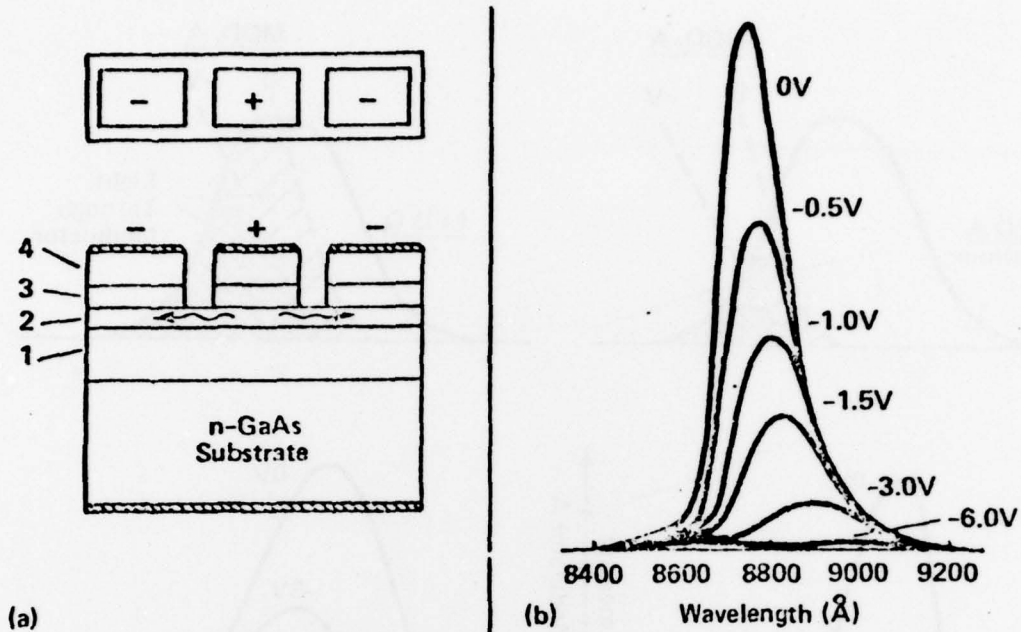


FIGURE 23. (a) Top and Side Views of Integrated Emitter-Modulator Design. Positive bias (+) indicates the single LED emitter and negative bias (-) indicates the two modulator sections. Layers are as described in Figure 20 with layer 2 being n-type. (b) Typical spectra taken after light passes through one of the modular arms biased at the indicated values. Guiding layer 2 has $N_D \approx 10^{16} \text{ cm}^{-3}$ and overall length 1.1 mm. (From reference cited in Footnote 45.)

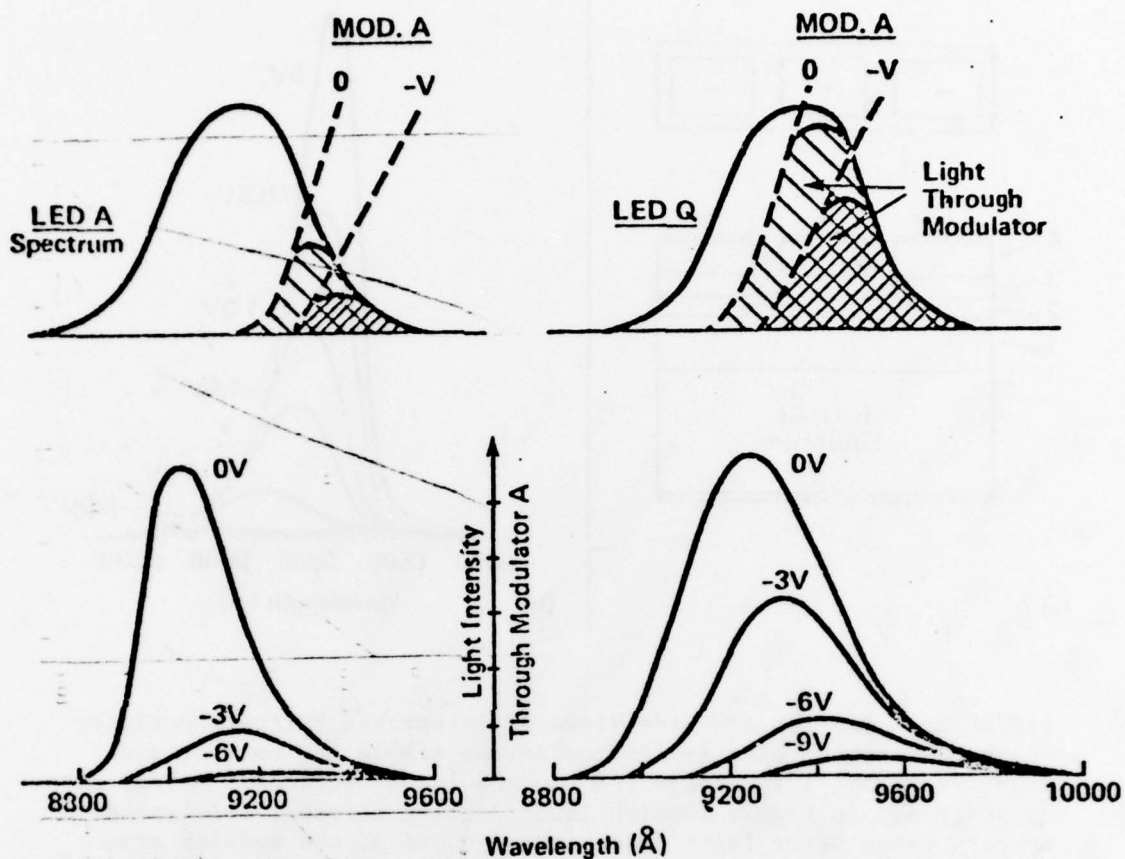


FIGURE 24. Top: Relative Positions of Transmission Edge of Modulator A at Biases of 0 and -V Within the Light Spectrum of LED A (From Same Wafer as Modulator A) and of LED Q (From Different Wafer) Chosen so That Large Portion of Light Passes Through Modulator at $V = 0$. Single and double crosshatching represent light transmitted through A biased at voltages of 0 and -V, respectively. Bottom: Actual experimental data for modulator A of Figure 20 at $V = 0, -3, -6, -9$ volts. (From reference cited in Footnote 45.)

Bell-Northern also tested the EA device to see how well it worked as a photodetector. Figure 25(a) shows a four-section photodetector device which was fabricated in the same way as the LED and EA modulator on the same substrate. Light is coupled into the waveguide (layer 2) of this device and each section, A, B, C, D, is biased successively more negatively than the previous one. This leads to absorption edges at successively lower photon energies, and the absorption edge as a function of photon energy will look like that shown in Figure 25(b). As can be seen by the absorption edge shown in Figure 25(b) there is a spectral overlap of the photocurrent response of each of the sections. In order that each section would have a unique spectral response a threshold circuit was designed so that amplifier A (Figure 25(a)) would respond only when the voltage across R exceeded the threshold level. Using this technique, experimental data are shown in Figure 26 for three sections and four sections of the photodetector. If the external threshold circuits were set to respond to voltages produced when photocurrents greater than the horizontal dashed lines flowed through R then a unique set of wavelengths would be detected in each circuit. The bandwidths of each section would vary from 170 to 440 Å for this particular device.

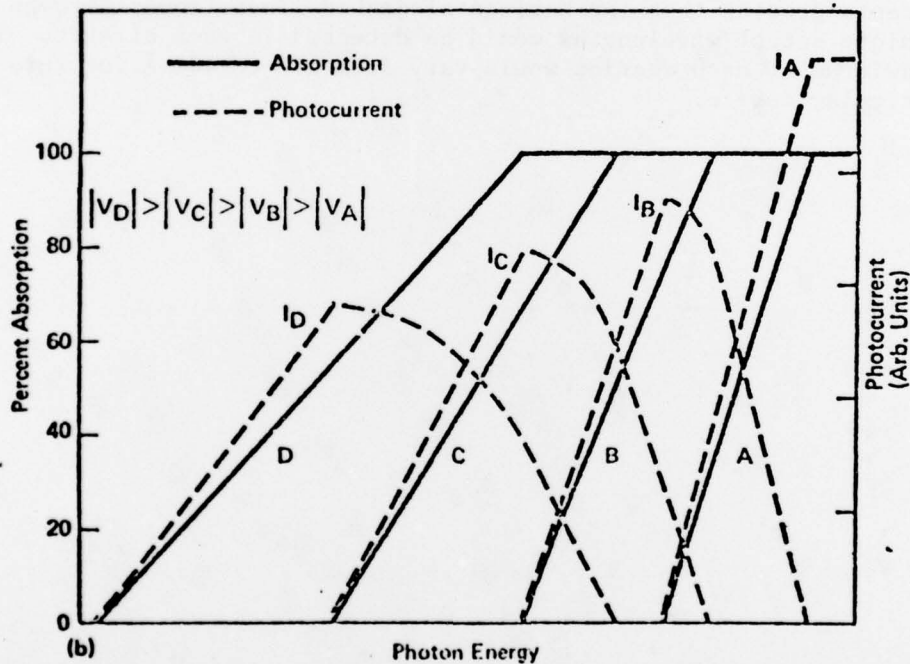
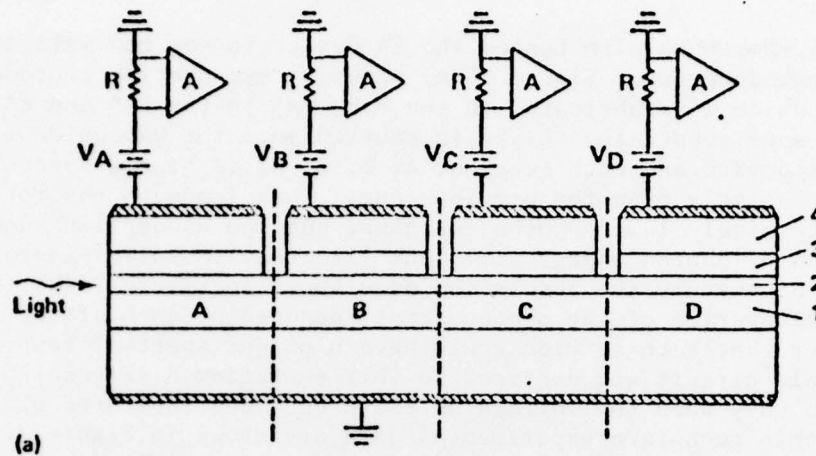


FIGURE 25. (a) Side View of Four-Section Photodetector With Layers as Described in Figure 23. The various sections are biased successively more negatively so that $|V_D| > |V_C| > |V_B| > |V_A|$. In each section, a resistor R and amplifier A could be arranged to ensure circuit response only to a unique range of wavelengths (see discussion of Figure 26). (b) Absorption edge shifts in sections A, B, C, D (solid lines which assume decreasing slopes) and corresponding calculated photocurrents (dashed lines). Shifts in peak photocurrent response to lower photon energies can be seen. (From reference cited in Footnote 45.)

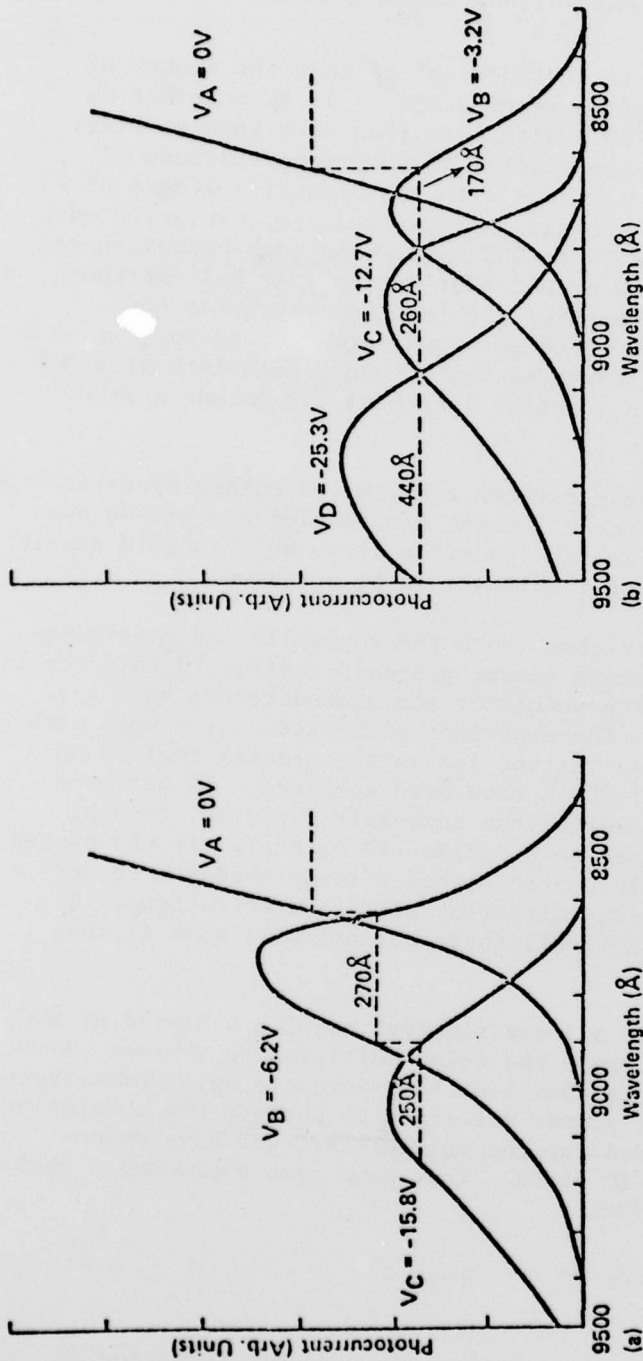


FIGURE 26. Experimental Photocurrents Measured in Which (a) Three Sections Are Biased or (b) Four Sections Are Biased at the Indicated Voltages. If the external circuits of Figure 25a were set to respond to photocurrents *above* the dashed horizontal lines, then each section would respond to a unique set of wavelengths with the indicated bandwidths. (From reference cited in Footnote 45.)

DISCUSSION, CONCLUSIONS, AND RECOMMENDATIONS

For device considerations it is important to know the amount of absorption edge shift with applied reverse bias. It is possible to achieve wavelength shifts of 700 Å with less than 20-V reverse bias. It is also possible for the photodetector to have edge spacings of 200 to 300 Å between adjacent sections with incremental voltages of -3 to -6 V. As the reverse bias voltage is increased the absorption edge gets less steep; the zero bias 10 to 90% absorption edge bandwidth can be made to less than 150 Å with proper fabrication. At Bell-Northern they have found that as the length of the junction waveguide gets longer the absorption edge bandwidth gets smaller. For example, a -3 V reverse bias with a junction length of 0.5 mm has a bandwidth of 170 Å and a -3 V reverse bias with a junction length of 1.3 mm has a bandwidth of 130 Å.

The response speeds of these devices are limited mainly by device capacitance and series resistance. Dymont has developed a proton bombardment technique⁴⁷ to decrease the junction area, which should enable multiplexing rates greater than 1 Gbit/sec to be achieved.

In conclusion, it has been shown both theoretically and experimentally that the color multiplexing scheme proposed earlier in this report is entirely feasible. Both the modulator and photodetector have been demonstrated experimentally. The experimental results agree well with those predicted theoretically. Extinction ratios greater than 30 dB and absorption edge shifts of 700 Å have been achieved. It has been shown that photodetectors in series can successfully detect several channels of information imposed on a single LED emitter. If the system is to consider temperature fluctuations then a study needs to be performed with the waveguide having different alloy concentrations. It has not yet been determined how well these devices will work if they are alloyed.

In view of the analytical and experimental results achieved at NWC, it is recommended that NWC pursue the color multiplexing scheme. Also, as has been presented here, personnel at Bell-Northern have demonstrated their capability to grow the proper materials to perform the modulating and detecting functions needed for the multiplexer, and have demonstrated an expertise in the IO field. They have also expressed a desire to cooperate and work with NWC.

⁴⁷ Dymont, J. C., and others. "Proton-Bombardment Formation of Stripe-Geometry Heterostructure Lasers for 300°K CW Operation," PROC IEEE, Vol. 60 (June 1972), pp. 726-28.